Frontiers in Bioscience Landmark

Front. Biosci. (Landmark Ed) **2026**; 31(9): 52155
https://doi.org/10.31083/FBL52155

Original Research

Extracorporeal Shock Wave Alleviates Knee Contracture in Rats by Inhibiting Hypoxia-Mediated Pyroptosis in Joint Capsular Fibroblasts

Quan-Bing Zhang[1,†], Xue-Ming Li[1,†], Xiu-Li Kan[1], Feng Wang[1], Lei Huo[2], A-Ying Liu[3], Mian Li[4], Qian-Qian Bao[5], Run Zhang[1], De-Ting Zhu[1], Zun-Yu Du[1], Jing Mao[1], Yun Zhou[1,*]

[1]Department of Rehabilitation Medicine, The Second Affiliated Hospital of Anhui Medical University, 230601 Hefei, Anhui, China
[2]Department of Rehabilitation Medicine, The Affiliated Hospital of the Neurology Institute in Anhui University of Chinese Medicine, 230000 Hefei, Anhui, China
[3]The Center for Scientific Research of the First Affiliated Hospital of Anhui Medical University, 230032 Hefei, Anhui, China
[4]Hefei Institute of Physical Sciences, Chinese Academy of Sciences, 230031 Hefei, Anhui, China
[5]The First Clinical Medicine College of Anhui Medical University, 230032 Hefei, Anhui, China
*Correspondence: zhoukeg@ahmu.edu.cn (Yun Zhou)
[†]These authors contributed equally.
Academic Editor: Elisa Belluzzi
Submitted: 22 March 2026 Revised: 21 June 2026 Accepted: 9 July 2026 Published: 18 September 2026

Abstract

Background: Joint immobilization frequently causes joint contracture, which may significantly impact an individual's quality of life. Consequently, extracorporeal shock wave (ESW) has been increasingly adopted to manage various bone and joint diseases. Our study investigated whether ESW therapy relieves knee contracture and if it mitigates the underlying hypoxia-induced pyroptosis of joint-capsule fibroblasts. **Methods:** A rat model of knee contracture was established through prolonged unilateral knee joint immobilization. Following the application of ESW, the levels of joint capsule fibrosis and cell pyroptosis were evaluated. During the immobilization phase, the NOD-like receptor protein 3 (NLRP3) specific inhibitor MCC950 was administered to assess its impact on pyroptosis levels. *In vitro*, hypoxia-induced rat knee joint synovial fibroblasts were exposed to hypoxia to induce myofibroblast differentiation. Hypoxia-inducible factor 1 alpha (HIF-1α) small interfering RNA was then used to inhibit HIF-1α expression, followed by the measurement of cell pyroptosis and fibrosis levels. **Results:** ESW intervention successfully mitigated knee contracture while decreasing pyroptosis and fibrosis in the joint capsule. Similarly, MCC950 treatment effectively inhibited both pyroptotic cell death and fibrotic tissue development within the capsule. Hypoxia induced the differentiation of synovial fibroblasts into myofibroblasts and increased pyroptosis. However, inhibiting HIF-1α expression mitigates these effects, leading to reduced pyroptosis and fibrosis in rat knee synovial fibroblasts. **Conclusions:** Hypoxic conditions promote pyroptosis in rat knee synovial fibroblasts and drive their differentiation into myofibroblasts, contributing to joint contracture. ESW therapy may alleviate joint contractures by partially inhibiting structural and cellular changes.

Keywords: joint contracture; extracorporeal shock wave; pyroptosis; fibroblasts

1. Introduction

Knee joint contracture often develops following trauma as a result of prolonged immobilization [1,2]. Because it frequently impacts laborers in sectors like transportation and construction, the condition poses a severe burden on public health systems, the medical economy, and the quality of life of patients. Therefore, exploring timely and effective treatments for knee contracture is of substantial academic and practical significance.

In rats, fixing the unilateral knee joint in extension restricts blood supply to articular tissues, inducing a hypoxic state within the joint capsule. This local hypoxia is recognized as a significant initiating mechanism for joint contracture [3]. Building upon this premise, mitigating joint capsular hypoxia through appropriate rehabilitation interventions could emerge as a viable therapeutic approach for joint contracture. Extracorporeal shock wave (ESW) is a widely used, non-invasive rehabilitation treatment. It is favored by both patients and medical professionals because it is safe, effective, and has minimal side effects [4,5,6]. ESW utilizes tensile and compressive stress to induce inter-tissue release, enhance capillary microcirculation, and promote cellular oxygen intake, effectively reversing local tissue hypoxia [7,8]. Our team previously demonstrated that ESW successfully treats joint contracture [9], though the specific mechanism requires further research.

Under hypoxic conditions, the expression of hypoxia-inducible factor 1 alpha (HIF-1α) is significantly upregulated [10,11]. Previous study have demonstrated that HIF-1α overexpression promotes NOD-like receptor protein 3 (NLRP3) activation [3]. Upon sensing relevant stimuli, NLRP3 and other inflammasomes utilize the adapter protein apoptosis-associated Speck-like protein (ASC) to activate caspase-1, which then cleaves gasdermin D (GSDMD),

separating its N-terminal domain from its C-terminal domain. This cleavage generates membrane pores that allow the release of intracellular contents and inflammatory cytokines, such as interleukin 1β (IL-1β) and IL-18. Previous studies have established that pyroptosis accelerates fibrosis in organs like the liver and kidney [12,13,14]. Because fibrotic remodeling shares fundamental pathological characteristics across different anatomical sites, pyroptosis may also promote joint capsule fibrosis during immobilization, thereby contributing to the development of joint contracture. Suppressing hypoxia-induced pyroptosis may serve as an additional mechanism by which ESW relieves joint contracture.

Considering the therapeutic mechanisms of ESW and the pathological alterations in the joint capsule, we propose that ESW mitigates joint contracture by alleviating local hypoxia and reducing fibrosis in the joint capsule. Building on previous research, this study evaluated the effect of ESW on knee contracture *in vivo*. Additionally, hypoxia-mediated pyroptosis in myofibroblasts was further investigated *in vitro*. Ultimately, these findings provide a theoretical framework for the clinical management of joint contracture. The experimental design is presented in Fig. 1.

2. Materials and Methods

2.1 Animals and Cells

Healthy, male Sprague–Dawley rats (3 months old, 250–300 g) from a closed-colony breeding source were provided by the Experimental Animal Center of Anhui Medical University. Additionally, rat knee joint synovial fibroblasts were purchased from iCell Bioscience Inc. (Shanghai, China) under the catalog number iCell-0135a. The cells were validated by short tandem repeat (STR) profiling and tested negative for mycoplasma. The current research was approved by the Institutional Animal Care and Use Committee of Anhui Medical University (No. LLSC20221126).

2.2 Induction of Joint Contracture

To induce knee contracture in rats, a molded aluminum splint was used to immobilize the unilateral hindlimb, extending from the groin to the base of the toes (Fig. 2A,B) [3].

2.3 Experimental Design

This study included both animal and cell experiments. Rats were randomly assigned to experimental groups using a computer-generated random number sequence.

In the first animal experiment, 24 Sprague–Dawley rats were divided into four equal groups of 6 rats to evaluate the effects of immobilization, natural recovery, and ESW intervention over an 8-week period. The rats were assigned to the following groups: Group M (immobilization) was immobilized for 4 weeks; Group NR (natural recovery) was immobilized for 4 weeks, followed by 4 weeks of natural recovery; Group E (ESW intervention) was immobilized for 4 weeks, followed by 4 weeks of ESW treatment; and Group C (control) was allowed free movement for the entire 8-week period.

ESW therapy was applied to the anterior joint capsule at twice-weekly intervals. Each session consisted of 2000 pulses delivered at a pressure of 1.5 bar and a frequency of 6 Hz (Fig. 2C,D). The ESW parameters were primarily based on our previous study [15], which confirmed the efficacy and safety.

In the second animal experiment, 18 Sprague–Dawley rats were equally distributed into three groups of 6 rats: Group C (control) moved freely for 4 weeks; Group M (immobilized model) was immobilized for 4 weeks; and Group MCC950 (intervention) was immobilized for 4 weeks with concurrent MCC950 treatment. Starting on the day of immobilization, the MCC950 group received 10 mg/kg intraperitoneal injections every 3 days. The MCC950 dosage was determined based on a previously reported regimen in rats [16].

A sample size of six animals per group was selected according to the 3R principle, guided by prior *in vivo* rat knee contracture research [15] and arthrogenic contracture power calculations. In the ESW experiment, Groups M and E demonstrated a mean difference of 9.42° with a pooled standard deviation (SD) of 3.10° (Cohen's d = 3.03). Power analysis showed that four animals per group yielded 80% power at a two-sided alpha level of 0.05, and increasing the sample size to six animals per group increased the power to 0.997. For the MCC950 experiment, the difference between the M and MCC950 groups was 7.45° with a pooled SD of 3.16° (Cohen's d = 2.36). While five animals per group were required for 80% power, using six animals per group achieved a statistical power of 0.957. Thus, 6 animals per group were considered sufficient to detect biologically meaningful changes while minimizing animal use.

In the first cell experiment, to confirm that hypoxia induces the differentiation of rat knee joint synovial fibroblasts into myofibroblasts, the knee joint synovial fibroblasts were cultured under either normoxic conditions or a 2% hypoxic atmosphere. The hypoxic treatments were sustained for 6, 12, and 24 h. Cells were divided into four groups: a normoxia group (cultured in normal oxygen environment for 24 h) and three hypoxia groups cultured for 6, 12, or 24 h. Following this, cell viability and alpha-smooth muscle actin (α-SMA) expression were evaluated.

In the second cell experiment, we investigated whether a hypoxic environment could promote pyroptosis and fibrosis. HIF-1α was silenced using small interfering RNA (siRNA) to evaluate its regulatory impact under hypoxic conditions. Pyroptosis and fibrosis-related protein levels were subsequently assessed to elucidate the involvement of HIF-1α in fibroblast responses to hypoxia. Cells were divided into four groups: Normoxia group (cultured in a standard oxygen environment for 24 h); Hypoxia group (cultured in hypoxic environment for 24 h); Hypoxia + siC-

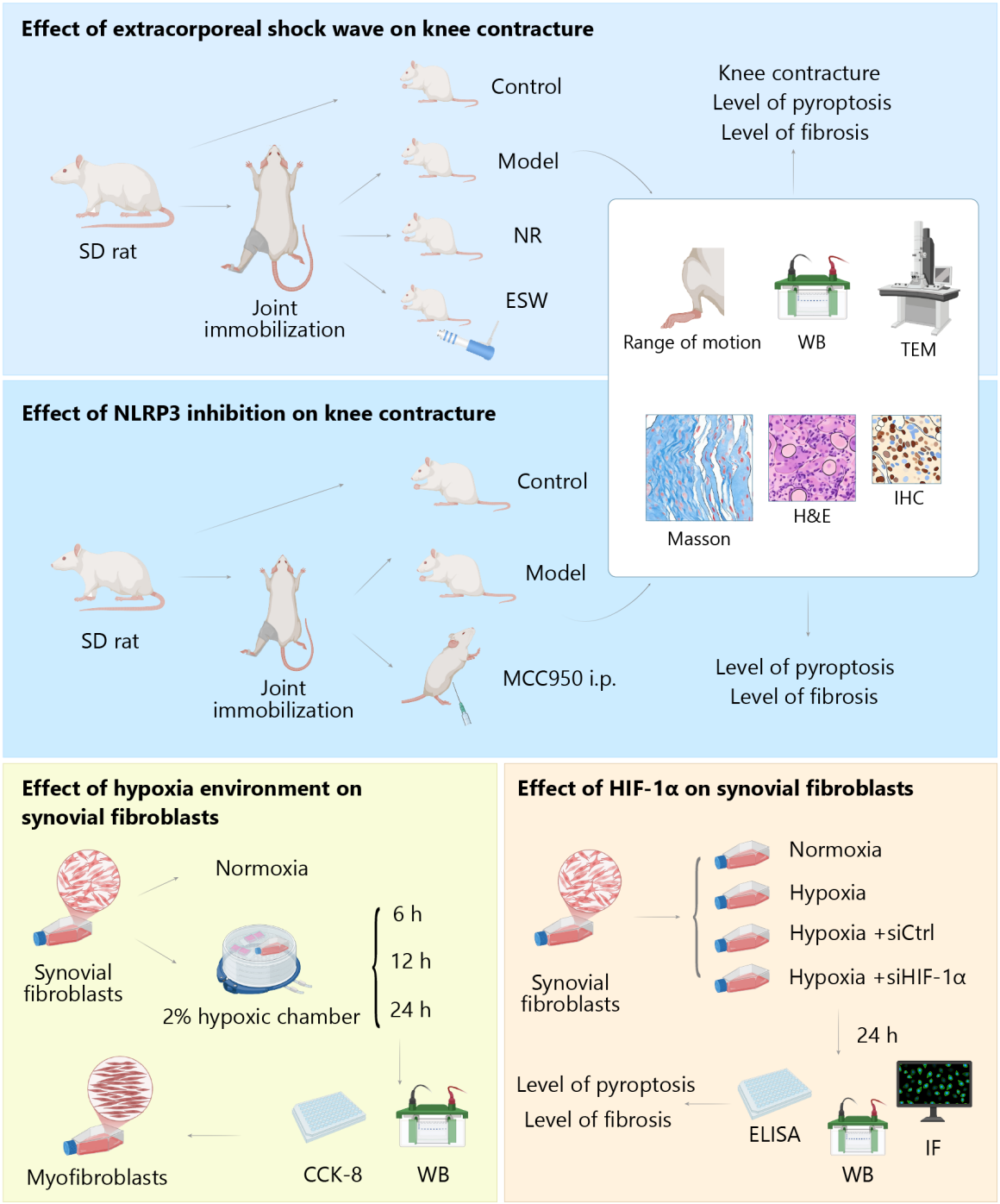

Fig. 1. Study design to assess the effect of NLRP3 inhibition on knee contracture that develops following joint immobilization in rats, focusing on hypoxia-induced pyroptosis and fibrosis. ESW, extracorporeal shock wave; CCK-8, Cell Counting Kit-8; ELISA, Enzyme-linked immunosorbent assay.

trl group (cultured in hypoxia for 24 h and simultaneously transfected with a negative control siRNA [Ctrl-siRNA]); and Hypoxia + siHIF-1α group (cultured in hypoxia for 24 h and simultaneously transfected with HIF-1α-siRNA). The investigators responsible for range of motion (ROM) measurements, histological analyses, and image quantifications were blinded to group allocation.

2.4 Evaluation of Joint Mobility Limitations

After each experiment, the rats were humanely euthanized with sodium pentobarbital overdose. The dose of sodium pentobarbital used for euthanasia was 120 mg/kg. Subsequently, the ROM of the rat knee joints was measured using a mechanical device developed by our research team (Patent No. ZL202120996643.1; Fig. 2E). Total and arthrogenic contractures were calculated as the difference

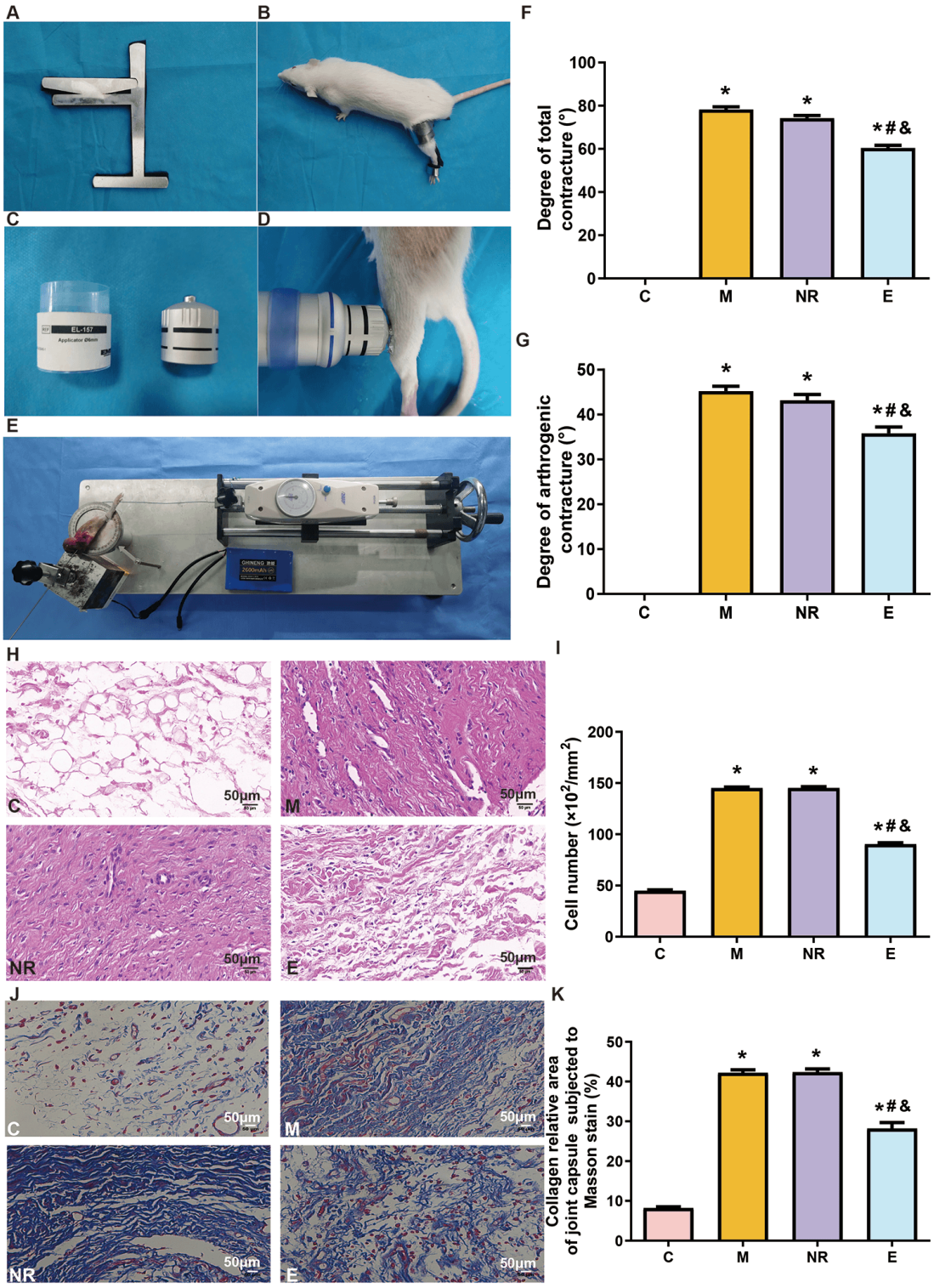

Fig. 2. ESW treatment led to a decrease in both cell count and collagen deposition within the anterior joint capsule. (A) Molded aluminum splint. (B) Establishment of a rat knee contracture model. (C) ESW therapy probe. (D) The rat received ESW intervention. (E) Measurement of joint ROM. (F) Quantitative analysis of the degree of total contracture. (G) Quantitative analysis of the degree of arthrogenic contracture. (H) Representative images of H&E staining. (I) Quantitative analysis of H&E staining. (J) Representative images of Masson staining. (K) Quantitative analysis of Masson staining. C, normal control group; M, model group; NR, natural recovery group; E, extracorporeal shock wave intervention group. Scale bar = 50 μm. Data are presented as mean ± SD (n = 6 rats per group). One-way ANOVA was used to assess the differences across multiple groups. $^{*}p < 0.05$ vs. Group C; $^{\#}p < 0.05$ vs. Group M; $^{\&}p < 0.05$ vs. group NR. ROM, range of motion; H&E, hematoxylin and eosin; ANOVA, analysis of variance.

in ROM between the control and experimental knees, evaluated immediately before and after myotomy, respectively.

2.5 Sample Preparation

Following removal of the anterior knee joint capsules and measurement of the ROM, the tissue samples were prepared for pathological and molecular analyses. During this process, a portion of the specimens was fixed overnight in 4% paraformaldehyde. The remaining specimens were flash-frozen in liquid nitrogen and stored at –80 °C.

2.6 Hematoxylin and Eosin Staining

Some specimens were subjected to hematoxylin and eosin (H&E) staining and examined under a microscope at a magnification of 400×. For each group, tissue sections from six different rats served as biological replicates. Three non-serial sections were prepared from each rat as technical replicates. For each section, six random fields of view magnification were captured and analyzed with Image Pro-Plus software (Image Pro-Plus 6.0, Media Cybernetics, Silver Spring, MD, USA). The average number of cells per square millimeter was then calculated in each group.

2.7 Masson Staining

Some specimens fixed in 4% paraformaldehyde were subjected to Masson staining and examined under 200× magnification. Six random regions per section were photographed and analyzed using Image ProPlus software (Media Cybernetics) to calculate the mean proportion of the blue area for each group. For each group, tissue sections from six different rats were used as biological replicates. Three non-serial sections were generated from each rat as technical replicates. For each section, six random fields of view at 200× magnification were photographed and quantified with Image ProPlus software (Image Pro-Plus 6.0, Media Cybernetics, Silver Spring, MD, USA) to evaluate collagen deposition. The mean collagen positive area ratio from the three sections was calculated for each biological replicate (n = 6 per group) and applied for statistical analysis.

2.8 Western Blotting

Western blotting was employed to assess protein expression levels. Total proteins were extracted using chilled Radio-Immunoprecipitation Assay (RIPA) lysis buffer containing Phenylmethylsulfonyl Fluoride (PMSF) (Beyotime, Beijing, China). Protein concentrations were subsequently quantified with a Bicinchoninic Acid (BCA) assay kit (Beyotime). Equal amounts from each sample pair were resolved using 10% sodium dodecyl sulfate polyacrylamide gel electrophoresis and electrotransferred to Polyvinylidene Difluoride (PVDF) membranes (Millipore, Bedford, MA, USA). The membrane was blocked in 5% skim milk in Tris-buffered saline containing Tween 20 (TBST) for 2 h at room temperature, followed by incubation overnight at 4 °C with rabbit anti-HIF-1α antibody (WL01607, Wanleibio; 1:1000), rabbit anti-NLRP3 antibody (bsm-61254R, Bioss; 1:2000), rabbit anti-GSDMD-N antibody (ab215203, Abcam; 1:1000), rabbit anti-GSDMD antibody (AF4012, Affinity; 1:1000), rabbit anti-caspase-1 antibody (AF5418, Affinity; 1:1000), rabbit anti-ASC antibody (DF6304, Affinity; 1:1000), rabbit anti-transforming growth factor beta 1 (TGF-β1) antibody (bsm-61027R, Bioss; 1:1000), rabbit anti-p-Smad3 antibody (bsm-52205R, Bioss; 1:1000), rabbit anti-Smad3 antibody (bsm-52224R, Bioss; 1:1000), rabbit anti-α-SMA antibody (bsm-52396R, Bioss; 1:500), and rabbit Glyceraldehyde-3-Phosphate Dehydrogenase (GAPDH) antibody (AF7021, Affinity; 1:5000). The next day, membranes were washed three times with TBST (10 min per wash) and incubated for 2 h at room temperature with horseradish peroxidase (HRP)-conjugated goat anti-rabbit Immunoglobulin G (IgG) (ab205718, Abcam; 1:5000). Following three additional 10-min washes, protein bands were visualized via enhanced chemiluminescence and quantified with ImageJ software (National Institutes of Health, Bethesda, MD, USA). Considering the limited volume of joint capsule tissue, lysates from six rats per group were pooled for western blotting analysis, with three independent technical replicates performed for densitometry. Three independent technical replicates were also applied in cell experiments. All representative bands were selected from these replicates.

2.9 Immunohistochemistry

In this study, immunohistochemistry (IHC) was performed to detect caspase-1, α-SMA and CD31 expression in positive cells. Joint capsule paraffin specimens were sectioned at a thickness of 5 μm. The slices were dewaxed in xylene I and xylene II solution for 20 min each, followed by rehydration in anhydrous alcohol I and anhydrous alcohol II for 10 min each. Then the slices were sequentially immersed in 95% and 90% ethanol solution for 5 min each, followed by antigen retrieval. Endogenous peroxidase activity was then quenched with hydrogen peroxide, and serum was applied to block non-specific antibody binding. Then the sections were incubated overnight at 4 °C with rabbit anti-caspase-1 antibody (AF5418, Affinity; 1:1000), rabbit anti-α-SMA antibody (bsm-52396R, Bioss; 1:200), or rabbit anti-CD31 antibody (bsm-10825R, Bioss; 1:200). Following phosphate-buffered saline (PBS) washes, the sections were incubated at 37 °C for 20 min with a peroxidase-conjugated goat anti-rabbit IgG-HRP (ab205718, Abcam; 1:1000). The diaminobenzidine (DAB) colorimetric method was employed for colorimetric visualization, and the sections were counterstained with hematoxylin. After dehydrating through graded ethanol and clearing in xylene, the slides were permanently mounted. For each group, tissue sections from six different rats served as biological replicates. From each rat, three non-serial sections were prepared as technical replicates. To evaluate caspase-1 and α-SMA protein expres-

sion, six random fields of view per section at 400× magnification were quantified using ImageJ, and the mean optical density from three sections was calculated for each biological replicate (n = 6 per group) for statistical analysis. To assess microvessel density (MVD) based on CD31 immunohistochemistry, six random fields of view per section at 400× magnification were captured and analyzed using Image ProPlus software (Image Pro-Plus 6.0; Media Cybernetics, Silver Spring, MD, USA), and the mean MVD was subsequently calculated for each group.

2.10 TEM

Joint capsule tissues were minced into 1 mm^3 fragments, rinsed with 0.1 M PBS, and fixed in 1% osmic acid for 1–2 h. Following graded dehydration, the specimens were embedded in epoxy resin and cut into ultra-thin sections. These sections were collected on copper grids and stained with lead citrate. Finally, ultrastructural images were acquired using the JEM-1400 transmission electron microscope (TEM) (JEOL, Tokyo, Japan). Joint capsule tissues from six rats per group served as biological replicates. To ensure representative findings, three copper grids per rat were prepared as technical replicates, and multiple fields were examined. Given that TEM was used for qualitative morphological assessment, the presented images represent one biological replicate per group.

2.11 Cell Culture and Model Differentiation

Rat knee joint synovial fibroblasts were cultured in a dedicated medium at 37 °C in a 5% CO_2 incubator. Cell density was observed under a microscope, and cultures were subcultured once they reached 80–90% confluency. Trypsin was added in a volume proportional to the dish size to completely cover the surface of the monolayer. The culture dish was incubated for 2 min and observed under an inverted microscope to assess cell detachment. When 70–80% of the cells were rounded and detached from each other, the flask was gently tapped to dislodge the remaining adherent cells. Complete growth medium containing serum was then added to neutralize the trypsin and terminate digestion. The cell suspension was centrifuged at 1000 rpmfor 3 min. The supernatant was discarded, and the cell pellet was resuspended in 9 mL complete culture medium. Then 3 mL cell suspension was transferred to a 10 cm culture dish containing 6 mL fresh complete medium and incubated. The hypoxia + siCtrl group and hypoxia +siHIF-1α group needed to be transfected with specific siRNA (General Bio Co., Ltd., China). Cells were transfected with siRNA using Lipofectamine 2000 (11668-019; Invitrogen, Thermo Fisher Scientific, Carlsbad, CA, USA) according to the manufacturer's protocol. The sequences used were as follows: HIF-1α siRNA, 5′-CCUCAAACCAGUUGAAUCUTT-3′ (forward) and 5′-AGAUUCAACUGGUUUGAGGTT-3′ (reverse); and Ctrl siRNA, 5′-UUCUCCGAACGUGUCACGUTT-3′ (forward) and 5′-ACGUGACACGUUCGGAGAATT-3′ (reverse).

2.12 Cell Counting Kit-8 Assay

Following trypsinization, cells were resuspended in complete medium and counted. A total of 5000 cells in 100 µL per well were seeded into 96-well plates, using three replicate wells per group. After adding 10 µL CCK-8 reagent to each well, the plates were incubated for 2 h in a humidified incubator. Absorbance was measured at 450 nm using a microplate reader.

2.13 Enzyme-Linked Immunosorbent Assay

Enzyme-linked immunosorbent assay (ELISA) kits (Shanghai Yapu Biotechnology Co., Ltd., Shanghai, China) were employed to evaluate the levels of IL-1β and IL-18. Samples and standards were added sequentially to microwells precoated with target-specific antibodies, followed by incubation with an HRP-labeled detection antibody. Following incubation and washing, 3,3',5,5'-Tetramethylbenzidine (TMB) substrate was added for chromogenic detection. Peroxidase catalyzed the oxidation of TMB into a blue intermediate, which shifted to a stable yellow product upon acidification. The intensity of this yellow color, which is directly proportional to the specimen's IL-1β or IL-18 concentration, was measured at 450 nm on a microplate reader. Analyte levels were then determined using a standard curve.

2.14 FAM-YVAD-FMK/PI Double Staining

Cells (4×10^5 cells) were seeded into 6-well plates containing coverslips and incubated overnight. After washing with PBS to remove debris and residual medium, 500 µL 5-carboxyfluorescein-Tyr-Val-Ala-Asp-fluoromethylketone (FAM-YVAD-FMK) working solution was gently added to the wells. Subsequently, the cells were incubated at 37 °C in the dark for 30 min and washed 2–3 times with PBS. Subsequently, 500 µL PI working solution was added, and the cells were incubated for 15 min at room temperature. After staining, the cells were washed once with PBS, fixed in 4% paraformaldehyde for 15–20 min, and rinsed 2–3 times with PBS. Finally, an appropriate amount of mounting medium was added to prepare a cell smear. Pyroptosis-positive cells exhibiting dual green and red fluorescence were visualized via fluorescence microscopy. The number of positive cells was quantified across three randomly selected fields of view.

2.15 Statistical Analyses

Statistical analyses were performed with SPSS 22.0 software (IBM Corp., Armonk, NY, USA). The data are presented as the mean ± SD. One-way analysis of variance (ANOVA) was used to assess the differences across multiple groups. If significant differences were detected, the

Bonferroni test or Tamhane T2 test was applied to perform pairwise comparisons. $p < 0.05$ was considered statistically significant.

For quantitative correlation analysis, group-level means from both *in vivo* experiments yielded seven distinct data points: C, M, NR, and E (from the ESW experiment); and C, M, and MCC950 (from the MCC950 experiment). Pyroptosis-related molecular status was defined using the mean GSDMD-N/GAPDH ratio, whereas contracture and fibrosis severity were represented by the means of arthrogenic contracture and Masson collagen deposition, respectively.

3. Results

3.1 ESW Therapy Improves Total and Arthrogenic Contracture

The outcomes of total contracture and arthrogenic contracture are presented in Fig. 2F,G. Compared with Group C, Group M showed a markedly greater degree of contracture ($p < 0.05$). Following 4 weeks of unrestricted movement after a 4-week immobilization period, both total and arthrogenic joint contractures were markedly greater in Group NR than in Group C ($p < 0.05$). Group E showed a significantly lower degree of contracture than Groups NR and M ($p < 0.05$), though contractures were still higher than in Group C ($p < 0.05$).

3.2 ESW Treatment Decreases Both Cell Count and Collagen Deposition Within the Anterior Joint Capsule

The results of H&E staining are shown in Fig. 2H,I. Following 4 weeks of immobilization, cell proliferation significantly increased ($p < 0.05$). While the NR group showed a significant increase compared to Group C ($p < 0.05$), it did not significantly differ from the M group ($p > 0.05$). By contrast, the E group exhibited a significant decrease compared to both the M and NR groups ($p < 0.05$), though its cell count remained above normal baseline levels ($p < 0.05$).

As shown in the Masson staining results (Fig. 2J,K), Group M exhibited a statistically significant increase in collagen deposition after 4 weeks of immobilization ($p < 0.05$). Collagen deposition in the NR group remained above baseline ($p < 0.05$). There was no significant difference in collagen deposition between the NR and M groups ($p > 0.05$). However, Group E showed a significantly lower level of collagen deposition than both the M and NR groups ($p < 0.05$).

3.3 ESW Therapy Downregulates HIF-1α Protein Expression in the Anterior Joint Capsule

As shown in Fig. 3A,B, HIF-1α protein levels significantly increased after 4 weeks of immobilization. Group NR exhibited notably higher HIF-1α expression than Group C ($p < 0.05$), but displayed no significant difference compared to Group M ($p > 0.05$). The levels of HIF-1α in the anterior joint capsule in Group E were significantly decreased relative to Group M and Group NR ($p < 0.05$ for both). Conversely, Group E showed no statistical difference in protein levels compared to Group C ($p > 0.05$).

3.4 ESW Therapy Downregulates Cell Pyroptosis in the Anterior Joint Capsule

Fig. 3 illustrates the varying expression levels of pyroptosis-associated proteins across the different groups, with the Western blot results detailed in Fig. 3A,C–G. Protein expression of NLRP3, GSDMD-N, GSDMD, ASC, and caspase-1 was statistically elevated in Group M relative to Group C ($p < 0.05$). After 4 weeks of immobilization followed by 4 weeks of free activity, the protein levels of these molecules were significantly higher than in Group C ($p < 0.05$); however, they did not significantly differ from Group M ($p > 0.05$). Protein levels of the targeted molecules in Group E were significantly decreased compared to Groups M and NR ($p < 0.05$). Compared to Group C, the expression levels of NLRP3, GSDMD-N, GSDMD, and ASC were marginally elevated in Group E compared to Group C ($p > 0.05$), while caspase-1 expression was statistically higher ($p < 0.05$).

IHC results (Fig. 3H,I) revealed that caspase-1 expression was significantly upregulated in Group M compared to Group C ($p < 0.05$). Following 4 weeks of immobilization and an additional 4 weeks of unrestricted activity, the protein levels of caspase-1 in Group NR were notably higher than those in Group C ($p < 0.05$). caspase-1 protein levels in the anterior joint capsule showed no significant difference between Group M and Group NR ($p > 0.05$); however, levels in Group E were significantly lower than in Groups M and NR ($p < 0.05$ for both). Conversely, Group E showed significantly higher caspase-1 expression than Group C ($p < 0.05$).

IHC results of CD31 (Fig. 3J,K) indicated that MVD in the anterior joint capsule was significantly increased in Group M relative to Group C ($p < 0.05$). Notably, Group NR maintained high MVD levels comparable to Group M, showing no statistical significance ($p > 0.05$). After 4 weeks of ESW intervention (Group E), MVD was markedly increased compared to Groups C, M and NR ($p < 0.05$).

TEM revealed intact fibroblast cell membranes in the anterior joint capsule of Group C (Fig. 3L). By contrast, Groups M and NR exhibited ruptured cells and leaked contents. While Group E showed less membrane damage and leakage than Group NR, its cell membrane integrity remained inferior to that of Group C.

3.5 ESW Therapy Downregulates Activation of the Transforming Growth Factor Beta 1/Smad3 Signaling Pathway in the Anterior Joint Capsule

Fig. 4 shows the protein expression levels of key TGF-β1/Smad3 pathway proteins, with the Western blotting results shown in Fig. 4A–E. Compared to Group C, Group M showed significantly elevated levels of TGF-β1, α-SMA,

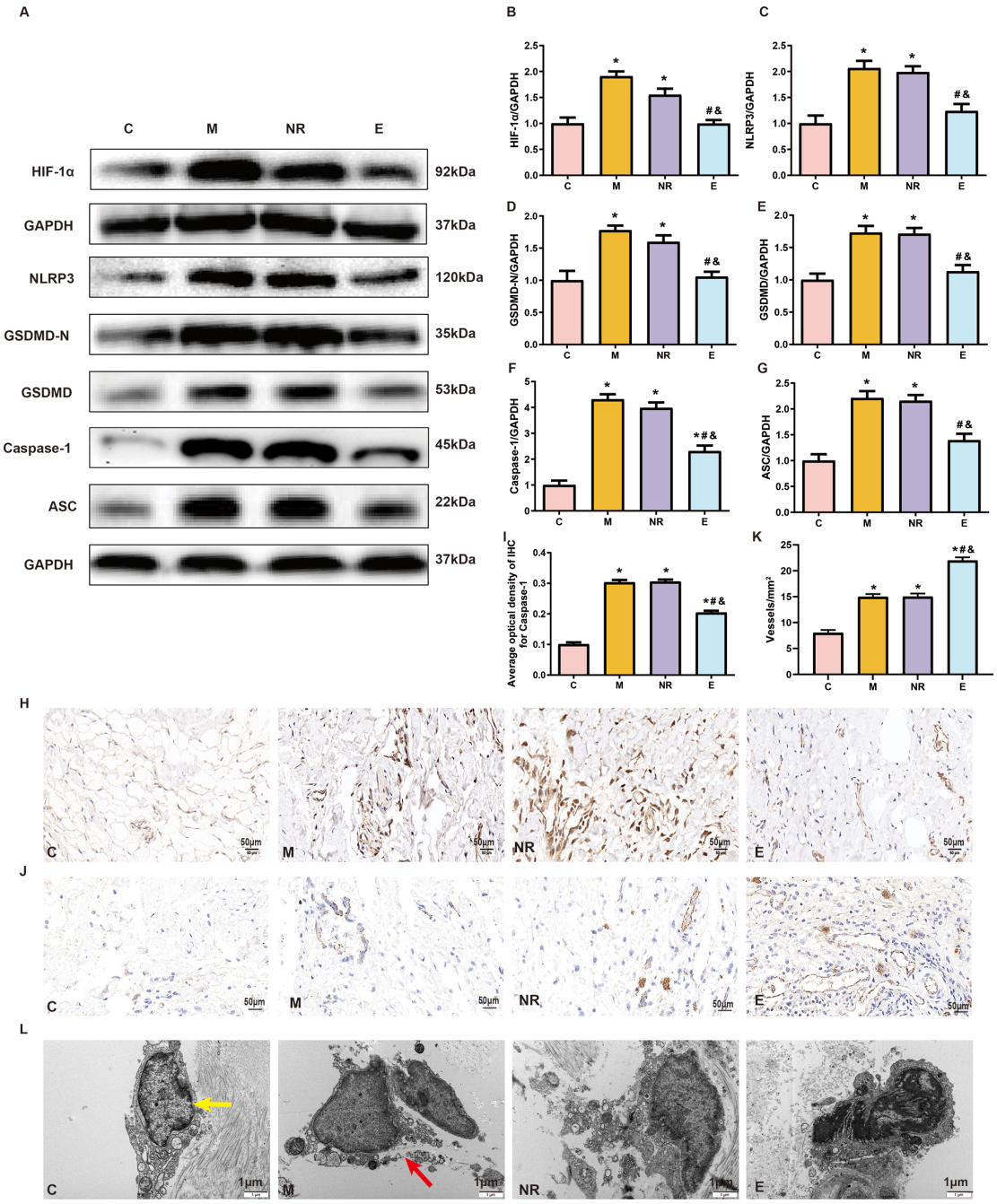

Fig. 3. ESW alleviated the overactivation of pyroptosis in the anterior joint capsule. (A) Representative Western blot images of HIF-1α, NLRP3, GSDMD-N, GSDMD, caspase-1, and ASC. (B) Western blot analysis and densitometric quantification of HIF-1α. (C) Western blot analysis and densitometric quantification of NLRP3. (D) Western blot analysis and densitometric quantification of GSDMD-N. (E) Western blot analysis and densitometric quantification of GSDMD. (F) Western blot analysis and densitometric quantification of caspase-1. (G) Western blot analysis and densitometric quantification of ASC. (H) Representative IHC images of caspase-1. Scale bar = 50 μm. (I) IHC quantification of caspase-1. (J) Representative IHC images of CD31. Scale bar = 50 μm. (K) IHC quantification of CD31. (L) Representative TEM images of anterior joint capsule fibroblasts in the C, M, NR, and E groups. Scale bar = 1 μm. C, normal control group; M, model group; NR, natural recovery group; E, extracorporeal shock wave intervention group. The yellow arrow shows the nucleus, and the red arrow shows the broken pores in the cell membrane. Data are presented as mean ± SD (n = 6 rats per group). One-way ANOVA was used to assess the differences across multiple groups. $^{*}p < 0.05$ vs. Group C; $^{\#}p < 0.05$ vs. Group M; $^{\&}p < 0.05$ vs. Group NR. HIF-1α, hypoxia-inducible factor 1 alpha; NLRP3, NOD-like receptor protein 3; GSDMD, gasdermin D; ASC, apoptosis-associated Speck-like protein; IHC, immunohistochemistry; TEM, transmission electron microscope; ANOVA, analysis of variance.

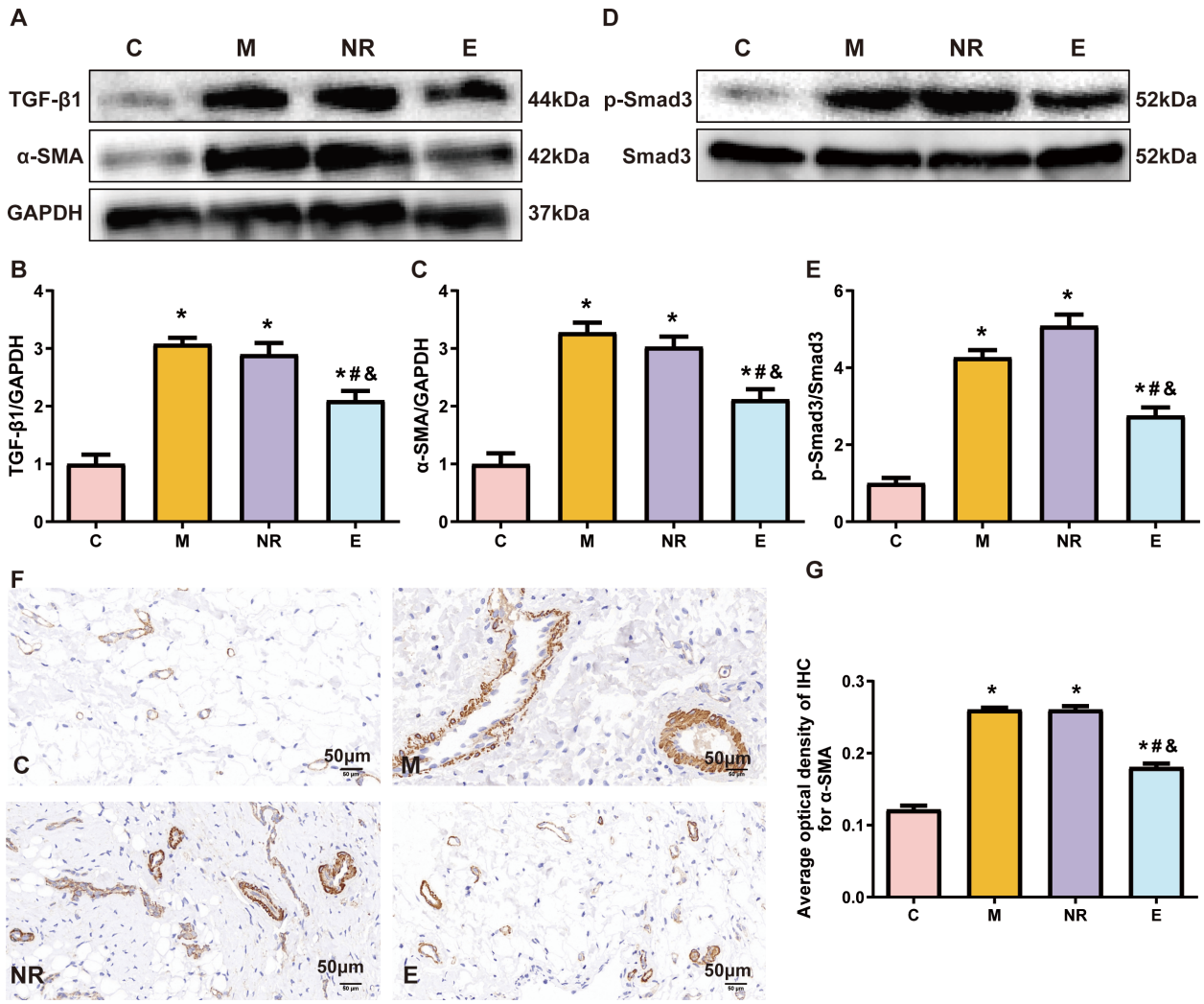

Fig. 4. ESW alleviated activation of TGF-β1/Smad3 signaling in the anterior joint capsule. (A) Representative Western blot images of TGF-β1, α-SMA. (B) Western blot analysis and densitometric quantification of TGF-β1. (C) Western blot analysis and densitometric quantification of α-SMA. (D) Representative Western blot images of p-Smad3. (E) Western blot analysis and densitometric quantification of p-Smad3. (F) Representative IHC images of α-SMA. Scale bar = 50 μm. (G) IHC quantification of α-SMA. C, normal control group; M, model group; NR, natural recovery group; E, ESW intervention group. Data are presented as mean ± SD (n = 6 rats per group). One-way ANOVA was used to assess the differences across multiple groups. $^{*}p < 0.05$ vs. Group C; $^{\#}p < 0.05$ vs. Group M; $^{\&}p < 0.05$ vs. Group NR. TGF-β1, transforming growth factor beta 1; α-SMA, alpha-smooth muscle actin; p-Smad3, phosphorylated Smad3; Smad3, mothers against decapentaplegic homolog 3; ANOVA, analysis of variance.

and phosphorylated Smad3 (p-Smad3) ($p < 0.05$). There was no significant difference in expression of the aforementioned molecules in Group NR compared to Group M ($p > 0.05$). However, Group E showed significantly reduced expression of these fibrotic markers compared to both Group M and Group NR ($p < 0.05$).

The IHC results, presented in Fig. 4F,G, revealed that the expression levels of α-SMA in Group M were statistically higher than those in Group C ($p < 0.05$). Furthermore, the expression of α-SMA in Group NR remained significantly elevated compared to Group C ($p < 0.05$). The expression levels of α-SMA in Group NR showed no significant difference compared to Group M ($p > 0.05$). However, levels in Group E were significantly lower than those in both Group M and Group NR ($p < 0.05$ for both). Furthermore, α-SMA expression in Group E was significantly higher than that in Group C ($p < 0.05$).

3.6 MCC950 Alleviates Total and Arthrogenic Contracture

The severity of joint contracture is illustrated in Fig. 5A,B. After 4 weeks of fixation, Group M exhibited a significant increase in contracture ($p < 0.05$). Co-administration of MCC950 during immobilization significantly reduced this contracture compared to Group M ($p < 0.05$), although levels remained higher than in Group C ($p < 0.05$).

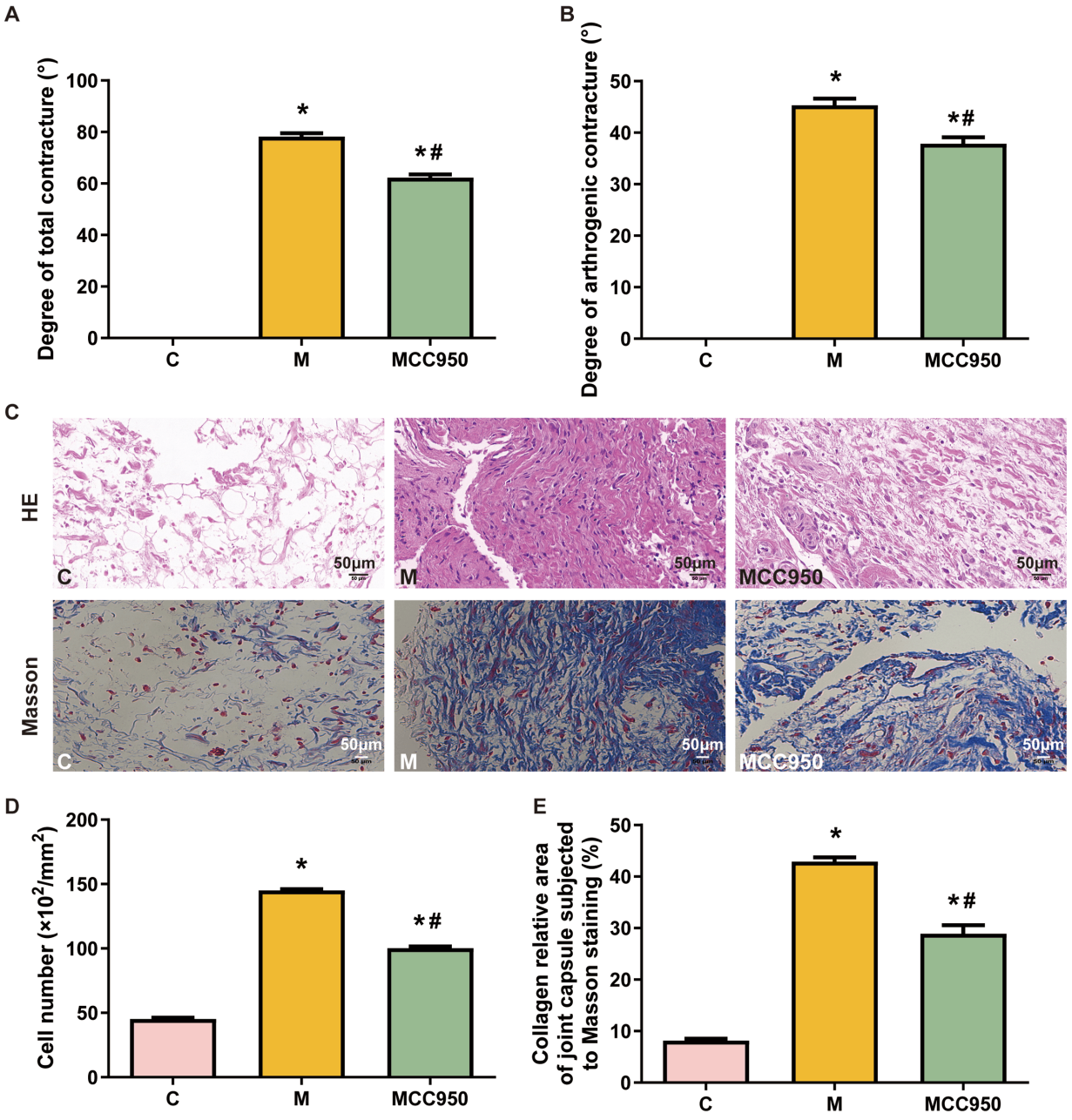

Fig. 5. MCC950 alleviated joint contracture and joint capsule fibrosis. (A) Quantitative analysis of the degree of total contracture. (B) Quantitative analysis of the degree of arthrogenic contracture. (C) Representative images of H&E and Masson staining. Scale bar = 50 μm. (D) Quantitative analysis of H&E staining. (E) Quantitative analysis of Masson staining. C, normal control group; M, model group; MCC950, MCC950 intervention group. Data are presented as mean ± SD (n = 6 rats per group). One-way ANOVA was used to assess the differences across multiple groups. $^{*}p < 0.05$ vs. Group C; $^{\#}p < 0.05$ vs. Group M. ANOVA, analysis of variance.

3.7 MCC950 Decreases Both Cell Count and Collagen Deposition Within the Anterior Joint Capsule

As shown in Fig. 5C–E, cell counts and collagen deposition were evaluated in the anterior joint capsule. Cell numbers were significantly higher in Group M than in Group C ($p < 0.05$). Treatment with MCC950 during fixation significantly attenuated the increase in cellularity ($p < 0.05$), but cell counts remained significantly elevated compared to Group C ($p < 0.05$).

Four weeks of immobilization significantly increased collagen deposition ($p < 0.05$). Simultaneous MCC950 treatment during this fixation period mitigated this effect ($p < 0.05$). However, the MCC950 group still showed a significantly higher degree of collagen deposition compared to Group C ($p < 0.05$).

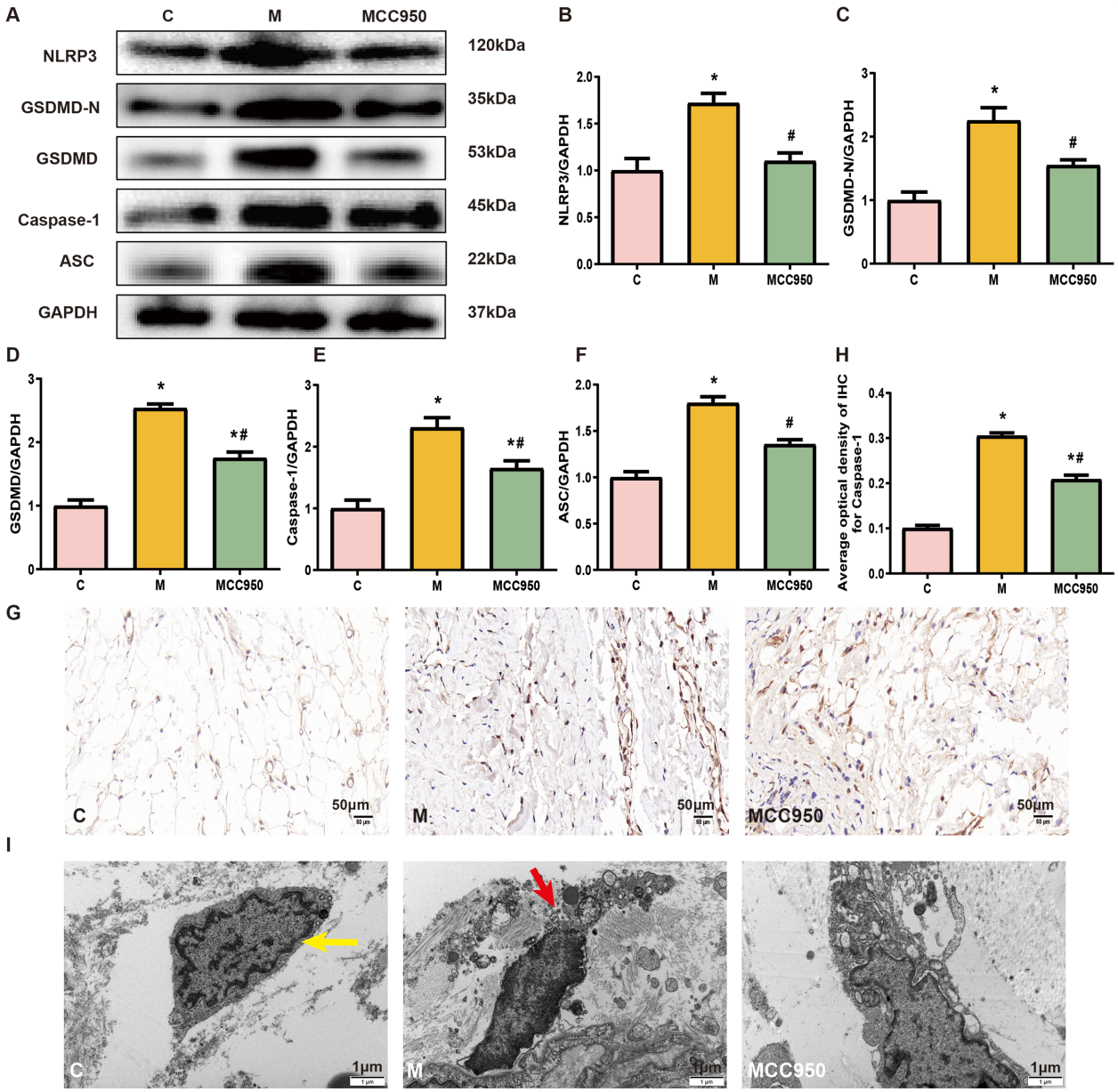

Fig. 6. MCC950 alleviated the overactivation of pyroptosis in the anterior joint capsule. (A) Representative Western blot images of NLRP3, GSDMD-N, GSDMD, caspase-1, and ASC. (B) Western blot analysis and densitometric quantification of NLRP3. (C) Western blot analysis and densitometric quantification of GSDMD-N. (D) Western blot analysis and densitometric quantification of GSDMD. (E) Western blot analysis and densitometric quantification of caspase-1. (F) Western blot analysis and densitometric quantification of ASC. (G) Representative IHC images of caspase-1. Scale bar = 50 μm. (H) IHC quantification of caspase-1. (I) Representative TEM images of normal rats. The yellow arrow shows the nucleus, and the red arrow shows the broken pores in the cell membrane. Scale bar = 50 μm. C, normal control group; M, model group; MCC950, MCC950 intervention group. Data are presented as mean ± SD (n = 6 rats per group). One-way ANOVA was used to assess the differences across multiple groups. $^{*}p < 0.05$ vs Group C; $^{\#}p < 0.05$ vs. Group M. ANOVA, analysis of variance.

3.8 MCC950 Downregulates Cell Pyroptosis Level in the Anterior Joint Capsule

Western blot analysis (Fig. 6A–F) demonstrates the expression levels of pyroptosis-related proteins. In Group M, the protein levels of NLRP3, GSDMD-N, GSDMD, caspase-1, and ASC were markedly elevated compared to Group C ($p < 0.05$). Simultaneous MCC950 treatment during the fixation period significantly reduced expression of the aforementioned proteins compared to Group M ($p < 0.05$). However, GSDMD and caspase-1 levels in the MCC950 group remained notably higher than in Group C ($p < 0.05$). Moreover, the MCC950 group showed slight, non-significant increases in NLRP3, GSDMD-N, and ASC expression relative to Group C ($p > 0.05$).

Immunohistochemical analysis (Fig. 6G,H) revealed that 4 weeks of immobilization significantly elevated caspase-1 expression ($p < 0.05$). Concurrent treatment with MCC950 during this period significantly attenuated caspase-1 levels compared to the immobilization-only group (Group M, $p < 0.05$). However, caspase-1 expression in the MCC950 remained significantly higher than normal baseline levels ($p < 0.05$).

Ultrastructural integrity was preserved in the anterior joint capsule fibroblasts of Group C (Fig. 6I). Conversely, Group M exhibited membrane rupture and subsequent leakage of cytoplasmic contents. Treatment with MCC950 substantially mitigated these pathological changes compared to Group M.

3.9 MCC950 Downregulates Activation of the TGF-β1/Smad3 Signaling Pathway in the Anterior Joint Capsule

Western blot analysis (Fig. 7A–D) revealed that Group M had significantly higher levels of TGF-β1, α-SMA, and p-Smad3 compared to Group C ($p < 0.05$). When MCC950 was administered during the fixation period, the MCC950 group showed significantly reduced levels of TGF-β1, α-SMA, and p-Smad3 compared to Group M ($p < 0.05$). However, these levels remained significantly higher than those in Group C ($p < 0.05$).

IHC (Fig. 7E,F) showed that α-SMA levels significantly increased in Group M compared to Group C after 4 weeks of immobilization ($p < 0.05$.). Co-treatment with MCC950 during immobilization significantly suppressed this increase, leading to lower expression levels in the MCC950 group than in Group M ($p < 0.05$). However, α-SMA expression in the MCC950 group remained significantly higher than in Group C ($p <0.05$).

3.10 Hypoxic Environment Induces the Differentiation of Rat Knee Synovial Fibroblasts Into Myofibroblasts

Fig. 8A,B demonstrate the impact of varying hypoxia durations on α-SMA expression in rat knee synovial fibroblasts. The results suggest that hypoxia conditions upregulate α-SMA expression, with the most pronounced increase in the 24-h exposure group. There was no significant difference in α-SMA expression between the Hypoxia-6h and Normoxia groups ($p > 0.05$), nor between the Hypoxia-12h and Hypoxia-6h groups ($p > 0.05$). However, levels significantly increased in the Hypoxia-12h group compared to Normoxia ($p < 0.05$). The Hypoxia-24h group showed the highest expression, which was significantly elevated compared to the Normoxia, Hypoxia-6h, and Hypoxia-12h groups ($p < 0.05$).

As shown in Fig. 8C, exposing synovial fibroblasts to hypoxia for 6, 12, and 24 h significantly reduced cell viability compared to normoxic controls ($p < 0.05$). Cell viability was significantly lower after 12 and 24 h of hypoxia compared to 6 h of exposure ($p < 0.05$). However, there was no significant difference in viability between the 12- and 24-h groups ($p > 0.05$).

3.11 HIF-1α siRNA Alleviates the Pyroptosis and Fibrosis Levels of Synovial Fibroblasts in Rat Knee Joints

Fig. 9A–G,L–O illustrate the effects of HIF-1α siRNA on pyroptosis and fibrosis-related proteins in rat knee synovial fibroblasts under hypoxic conditions. Compared to the normoxic control, the hypoxia group showed a significant increase in HIF-1α expression ($p < 0.05$). HIF-1α expression remained significantly elevated in the Hypoxia + siCtrl group compared to the Normoxia group ($p < 0.05$). However, HIF-1α protein levels showed no significant difference between the Hypoxia group and the Hypoxia + siCtrl group ($p > 0.05$). HIF-1α protein expression was significantly lower in the Hypoxia + siHIF-1α group than in the hypoxia-exposed groups (Hypoxia and Hypoxia + siCtrl) ($p < 0.05$). Despite this increase, HIF-1α levels were not significantly different from those in the Normoxia controls. ($p > 0.05$). Relative to the normoxia group, pyroptosis-related proteins (NLRP3, GSDMD-N, GSDMD, caspase-1, and ASC) were significantly upregulated in both the Hypoxia and Hypoxia + siCtrl groups ($p < 0.05$). Expression of the aforementioned proteins was significantly lower in the Hypoxia + siHIF-1α group than in the Hypoxia and Hypoxia + siCtrl groups ($p < 0.05$). However, these levels were still higher than those in the Normoxia group, but failed to reach statistical difference ($p > 0.05$). Compared to the Normoxia group, the Hypoxia and Hypoxia + siCtrl groups showed significantly elevated expression of fibrosis-related proteins TGF-β1, α-SMA, and p-Smad3 ($p < 0.05$). Knocking down HIF-1α (Hypoxia + siHIF-1α group) significantly reduced these protein levels compared to the Hypoxia and Hypoxia + siCtrl groups ($p < 0.05$), although they remained slightly higher than those in the Normoxia group ($p > 0.05$).

FAM-YVAD-FMK/PI double staining (Fig. 9H,I) revealed significantly more pyroptosis-positive cells in the Hypoxia and Hypoxia + siCtrl groups compared to the Normoxia group ($p < 0.05$). Silencing HIF-1α (Hypoxia + siHIF-1α) markedly reduced this hypoxia-induced pyroptosis, bringing the levels down close to Normoxia controls ($p < 0.05$).

ELISA (Fig. 9J,K) revealed that hypoxic conditions (Hypoxia and Hypoxia + siCtrl groups) caused a sharp increase in IL-1β and IL-18 expression levels compared to the Normoxia group ($p < 0.05$). By contrast, the Hypoxia + siHIF-1α group exhibited a marked reduction in the expression of both cytokines compared with the Hypoxia and Hypoxia + siCtrl groups ($p < 0.05$). Notably, however, these levels remained significantly higher than those observed under normoxic conditions ($p < 0.05$).

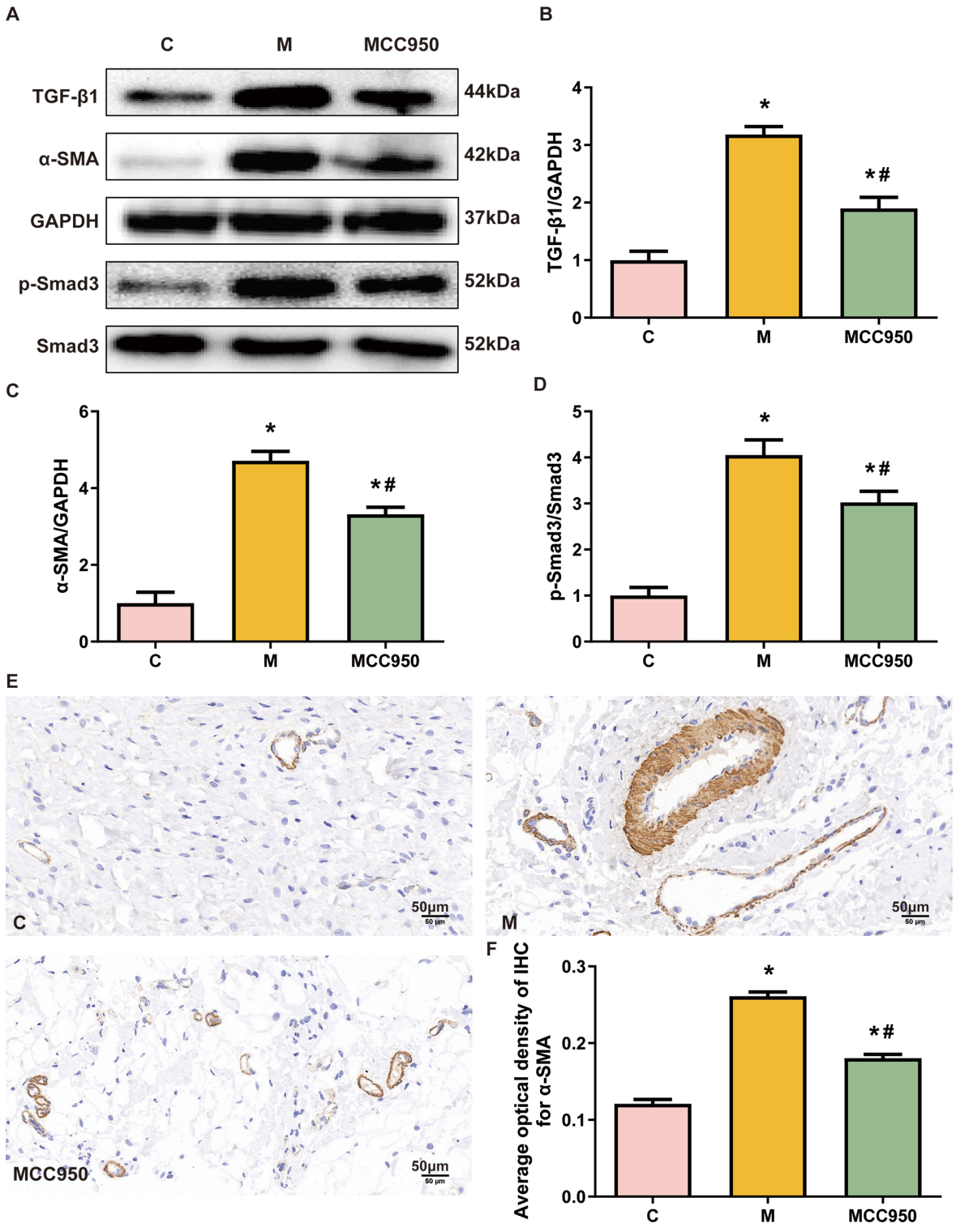

Fig. 7. MCC950 alleviated activation of the TGF-β1/Smad3 signaling pathway in the anterior joint capsule. (A) Representative Western blot images of TGF-β1, Smad3, p-Smad3 and α-SMA. (B) Western blot analysis and densitometric quantification of TGF-β1. (C) Western blot analysis and densitometric quantification of α-SMA. (D) Western blot analysis and densitometric quantification of p-Smad3. (E) Representative IHC images of α-SMA. Scale bar = 50 μm. (F) IHC quantification analysis of α-SMA. C, normal control group; M, model group; MCC950, MCC950 intervention group. Data are presented as mean ± SD (n = 6 rats per group). One-way ANOVA was used to assess the differences across multiple groups. $^{*}p < 0.05$ vs. Group C; $^{\#}p < 0.05$ vs. Group M. ANOVA, analysis of variance.

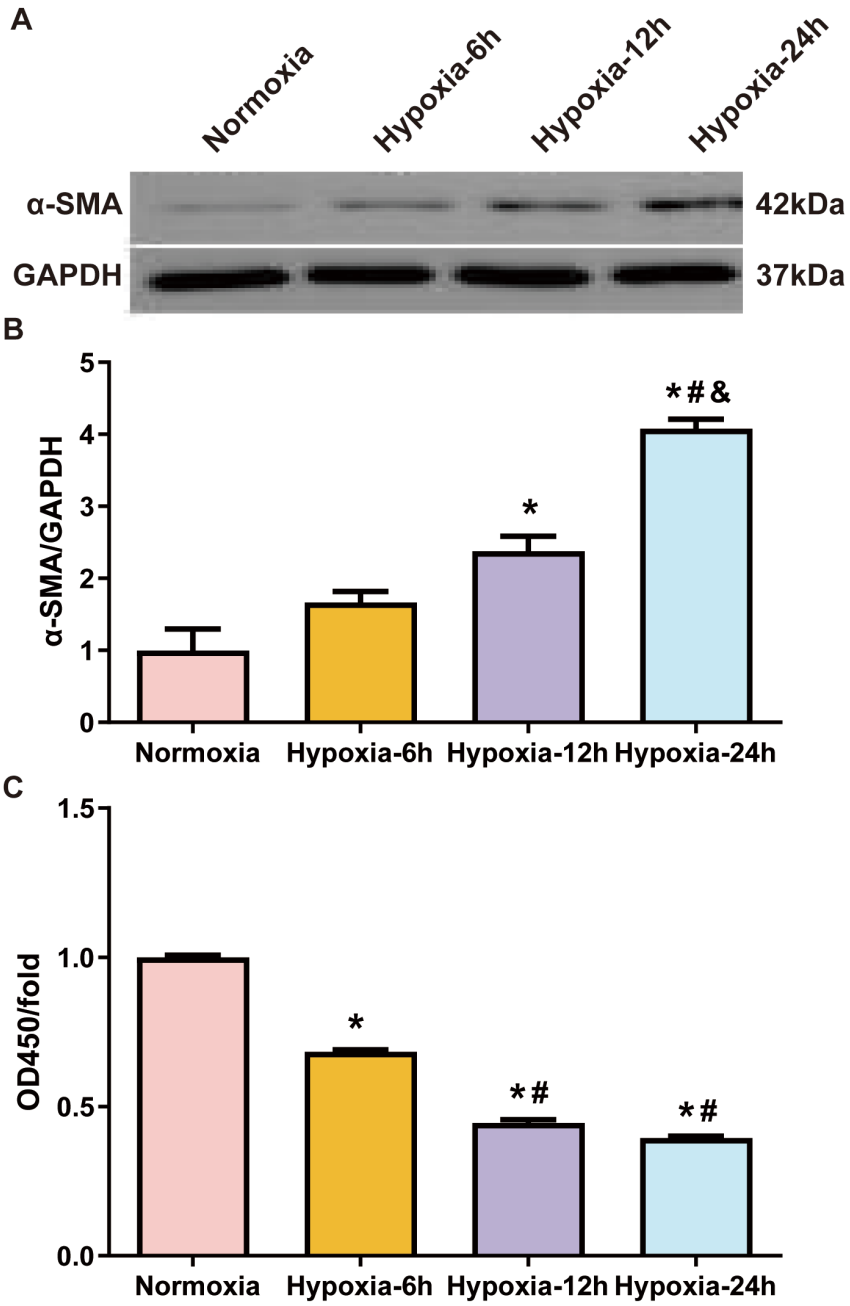

Fig. 8. Hypoxic environment induced the differentiation of rat knee synovial fibroblasts into myofibroblasts. (A) Representative Western blot images of α-SMA expression. (B) Quantitative analysis of α-SMA expression. (C) CCK-8 cell viability test results. Normoxia, fibroblasts cultured in normal oxygen concentration environment. The y-axis label "OD450/fold" indicates that the values are normalized fold changes derived from OD450 absorbance readings, and all raw OD450 values were normalized to the normoxia control group (set as 1.0). Three independent experiments were performed for the Western blot and CCK-8 assays. Hypoxia-6h, fibroblasts placed in 2% hypoxic chamber for 6 h; Hypoxia-12h, fibroblasts placed in 2% hypoxic chamber for 12 h; Hypoxia-24h, fibroblasts placed in 2% hypoxic chamber for 24 h. $^{*}p < 0.05$ vs. Normoxia group; $^{\#}p < 0.05$ vs. Hypoxia-6h group; $^{\&}p < 0.05$ vs. Hypoxia-12h group.

3.12 Association of Pyroptosis Activation With Contracture and Fibrosis

Using group-level mean values from the ESW and MCC950 *in vivo* experiments, we examined whether pyroptosis activation was linked to the severity of joint contracture and capsular fibrosis. Levels of GSDMD-N/GAPDH showed a perfect correlation with arthrogenic contracture (Spearman's rho = 1.000, permutation $p < 0.001$; Fig. 10A), and a strong positive correlation with Masson collagen deposition (Spearman rho = 0.955, permutation $p = 0.004$; Fig.

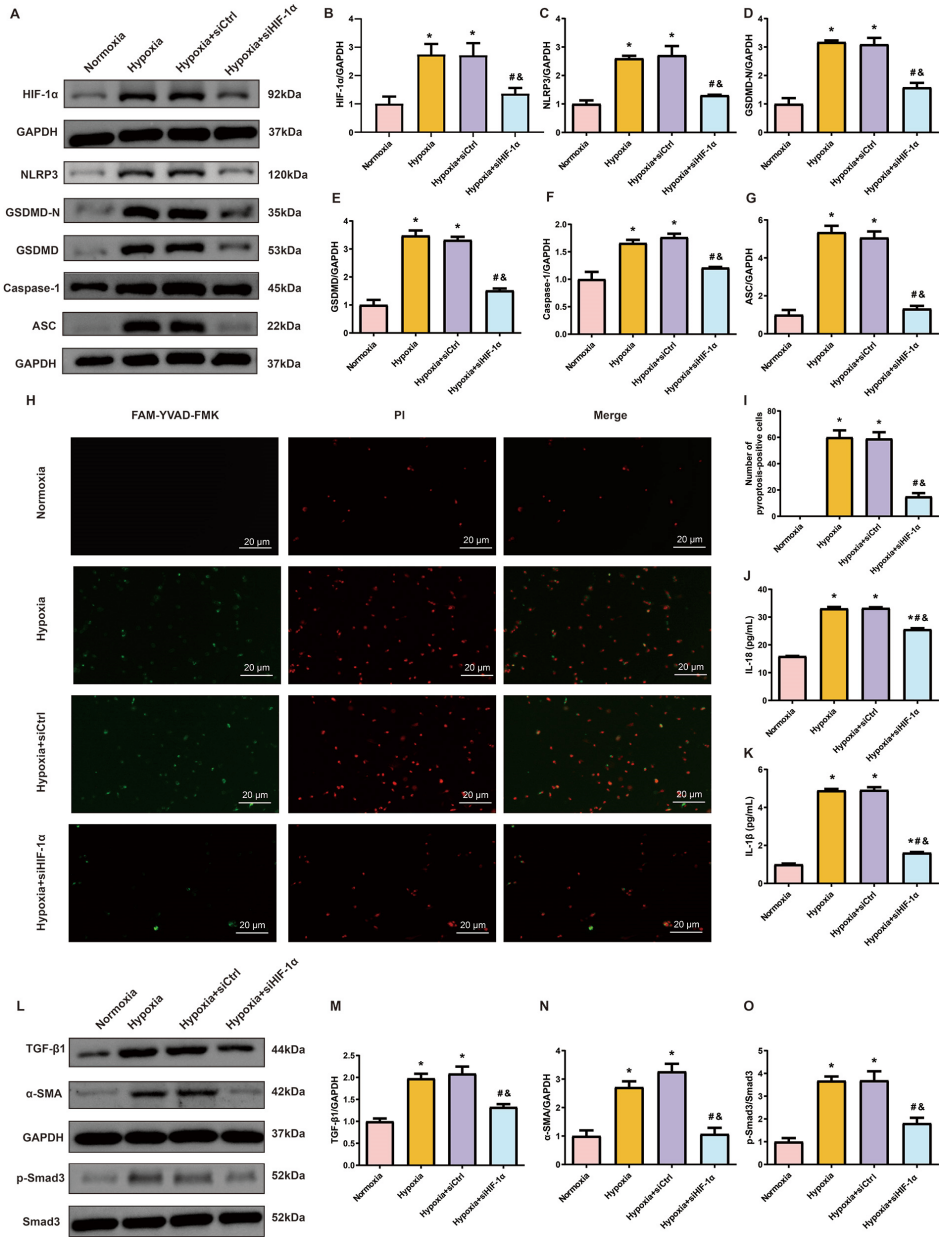

Fig. 9. HIF-1α siRNA attenuates hypoxia-induced pyroptosis and fibrotic responses in rat knee synovial fibroblasts. (A) Representative Western blot images of HIF-1α, NLRP3, GSDMD-N, GSDMD, caspase-1 and ASC. (B) Western blot analysis and densitometric quantification of HIF-1α. (C) Western blot analysis and densitometric quantification of NLRP3. (D) Western blot analysis and densitometric quantification of GSDMD-N. (E) Western blot analysis and densitometric quantification of GSDMD. (F) Western blot analysis and densitometric quantification of caspase-1. (G) Western blot analysis and densitometric quantification of ASC. (H) FAM-YVAD-FMK/PI double staining. Original magnification, ×100. Scale bar = 20 μm. (I) Quantitative analysis of FAM-YVAD-FMK/PI double staining. (J) Quantitative analysis of ELISA for IL-18. (K) Quantitative analysis of ELISA for IL-1β. (L) Representative Western blot images of TGF-β1, α-SMA and Smad3. (M) Western blot analysis and densitometric quantification of TGF-β1. (N) Western blot analysis and densitometric quantification of α-SMA. (O) Western blot analysis and densitometric quantification of p-Smad3. Normoxia, fibroblasts cultured in normal oxygen concentration environment; Hypoxia, fibroblasts placed in 2% hypoxic chamber for 24 hours; Hypoxia + siCtrl, fibroblasts placed in 2% hypoxic chamber for 24 hours and transfected with the negative control agent Ctrl-siRNA simultaneously; hypoxia +siHIF-1α, fibroblasts placed in 2% hypoxic chamber for 24 hours and transfected with HIF-1α-siRNA simultaneously. $^{*}p < 0.05$ vs. Group Normoxia; $^{\#}p < 0.05$ vs. Group Hypoxia; $^{\&}p < 0.05$ vs. Group "Hypoxia + siCtrl". FAM-YVAD-FMK/PI, 5-carboxyfluorescein-Tyr-Val-Ala-Asp-fluoromethylketone/propidium iodide; IL-18, Interleukin-18; IL-1β, Interleukin-1 beta.

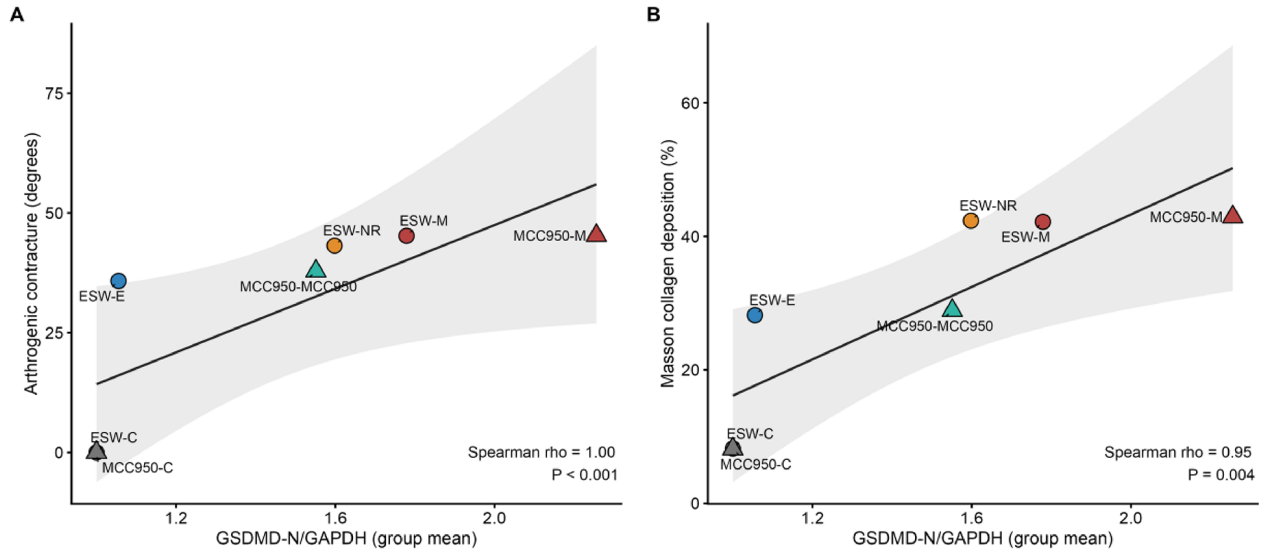

Fig. 10. Group-mean correlation between pyroptosis activation and the severity of contracture/fibrosis *in vivo*. (A) Correlation between GSDMD-N/GAPDH and arthrogenic contracture. (B) Correlation between GSDMD-N/GAPDH and Masson collagen deposition. Each point represents one experimental group mean from the ESW experiment (C, M, NR, and E) or the MCC950 experiment (C, M, and MCC950).

10B). These results indicate that heightened pyroptosis corresponds to more severe joint contracture and fibrotic tissue changes.

4. Discussion

Fibrosis of the joint capsule is a primary pathogenic mechanism in the development of joint contractures [2,17]. Consequently, the successful clinical management of joint contracture depends on timely and efficient targeted interventions directed at mitigating this fibrotic process. The defining feature of tissue fibrosis is the differentiation of fibroblasts into myofibroblasts. Inhibiting this transition is a promising therapeutic strategy for treating the condition [18]. In recent years, ESW therapy has emerged as a prominent physical therapy in rehabilitation medicine and sports medicine, offering significant therapeutic benefits for various soft tissue disorders [19,20]. Additionally, current research indicates that ESW effectively inhibits tissue fibrosis [21,22]. Recent studies demonstrate that ESW therapy has significant anti-fibrotic effects. A study by Ujiie et al. [21] showed that ESW effectively inhibits liver fibrosis in liver cirrhosis models. Similarly, Zhao et al. [22] found that ESW inhibits scar hyperplasia in animal models of ear thickening, indicating its potential to prevent fibrosis in epidermal tissues as well. In this study, we demonstrated that ESW therapy alleviates immobilization-induced knee joint contracture by inhibiting the HIF-1α/NLRP3-mediated pyroptosis pathway in joint capsular fibroblasts. These findings support and build upon existing research on the anti-fibrotic benefits of ESW for musculoskeletal disorders. For example, Sorg et al. [7] demonstrated that radial ESW reduces muscle fibrosis and contractures in rabbits by blocking the HIF-1α signaling pathway. Additionally, Stania et al. [6] highlighted the broad clinical application of ESW in treating Achilles tendinopathy. Our study complements these observations by demonstrating for the first time that ESW therapy effectively suppresses joint contracture by inhibiting NLRP3-driven pyroptosis—a mechanism previously unknown for ESW. These findings provide novel mechanistic insights into the anti-fibrotic effects of ESW and suggest that targeting the HIF-1α/NLRP3/pyroptosis axis could be a promising new therapeutic strategy.

The most reliable indicator of joint contracture is a measurable decrease in the joint's ROM [1,23,24]. In this study, after 4 weeks of aluminum splint fixation, the rat knee joints exhibited a significant reduction in mobility, indicating successful establishment of the joint contracture model. Four weeks of natural recovery following 4-week unilateral knee immobilization failed to yield significant improvements in ROM. These results indicate that ROM restrictions induced by immobilization do not recover spontaneously without timely rehabilitation. However, introducing 4 weeks of ESW can significantly improve joint mobility, demonstrating its efficacy in treating knee joint contracture. Meanwhile, joint ROM of the rats after immobilization and ESW was still markedly lower than that of normal rats, suggesting that joint mobility is not fully restored after ESW therapy. Thus, ESW should be combined with other treatments to ensure better rehabilitation treatment effects. Tissue fibrosis typically manifests as local chronic inflammation and excessive collagen fiber deposition, accompanied by an increase in inflammatory cells and active fibrob-

lasts [25]. In this study, joint immobilization induced cell proliferation, including inflammatory cells and fibroblasts, which did not resolve after 4 weeks of natural recovery. Conversely, 4 weeks of ESW significantly decreased the total cell count in the anterior joint capsule, suggesting that this intervention is an effective strategy for mitigating joint capsule fibrosis. Increased collagen deposition is a hallmark of tissue fibrosis [26,27]. In this study, we observed that immobilizing the rat knee joint in an extended position for 4 weeks markedly increased collagen levels, indicating the development of anterior joint capsule fibrosis. Notably, after 4 weeks of unrestricted recovery, this collagen accumulation showed no significant reduction. Notably, after 4 weeks of ESW intervention following 4 weeks of fixation, the level of collagen deposition was reduced, suggesting that ESW intervention has a significant therapeutic effect on relieving joint capsule fibrosis. These findings indicate that ESW may alleviate joint contracture, at least in part, by attenuating collagen deposition and reversing fibrotic changes within the knee joint capsule.

The development of joint capsule fibrosis involves complex molecular signaling. In our immobilization model, the TGF-β1/Smad3 pathway—a primary driver of tissue fibrosis—was markedly upregulated after 4 weeks. The elevated levels of TGF-β1, p-Smad3, and α-SMA provide evidence of this pathway's role in the fibrotic process. Molecular analysis following 4 weeks of unilateral knee immobilization and subsequent 4-week ESW revealed the downregulation of TGF-β1, phosphorylated Smad3, and α-SMA in the anterior joint capsule. ESW appears to mitigate joint contracture by suppressing this overactive fibrotic pathway.

During the immobilization process of rat knee joints, local tissues experience hypoxia, resulting in elevated HIF-1α levels—a potential trigger for joint contracture [28]. This increase in HIF-1α drives the upregulation of NLRP3, a key initiator of pyroptosis [29,30,31,32]. Consequently, NLRP3-mediated pyroptosis has been increasingly identified as a driver in various joint pathologies. Notably, Hong et al. [30] demonstrated that the ROS/GRK2/HIF-1α/NLRP3 pathway mediates pyroptosis in fibroblast-like synoviocytes in a model of inflammatory arthritis. Shi et al. [33] demonstrated that DDX3X/NLRP3/GSDMD pathway-mediated pyroptosis promotes pyroptosis and inflammatory injury in osteoarthritic chondrocytes. Our findings extend these observations to immobilization-induced joint contracture, a primarily mechanical fibrotic disorder, suggesting that the HIF-1α/NLRP3/pyroptosis axis may represent a shared pathological mechanism driving joint degeneration from both inflammatory and mechanical insults. Previous studies have suggested that local tissue hypoxia contributes to the progression of diseases, including myogenic contracture and ischemic injury to the limb [7,32]. This study innovatively investigated the pathomolecular alterations in the joint capsule following hypoxia. In this research, the protein levels of HIF-1α in the anterior joint capsule were elevated following immobilization. The abnormally upregulated expression of HIF-1α was suppressed by ESW, indicating that this intervention may act, at least in part, by improving tissue oxygen availability. To further determine whether ESW promotes angiogenesis and thereby relieves local hypoxia in the joint capsule, we performed CD31 immunohistochemistry. The results hinted that immobilization may induce a hypoxic microenvironment in the anterior joint capsule, triggering a compensatory angiogenic response that nevertheless failed to restore local oxygen homeostasis. In contrast, ESW intervention markedly enhanced microvascular density, indicating a pro-angiogenic effect beyond the intrinsic compensatory reserve. This ESW-mediated improvement in local perfusion likely relieves tissue hypoxia, thereby favoring the subsequent downregulation of pyroptosis. Collectively, these findings suggest that the therapeutic benefit of ESW may derive, at least in part, from its capacity to remodel the vascular niche and reestablish perfusion homeostasis in chronically stressed joint capsules. Consistent with the pro-fibrotic role of pyroptosis reported in other organs [34,35,36,37,38], our molecular analyses revealed the marked upregulation of pyroptosis-associated proteins in the joint capsule following immobilization. However, applying ESW downregulated these pyroptosis-related proteins in the anterior joint capsule. Meanwhile, TEM also showed that the fibroblast membranes in the anterior joint capsules of healthy rats remained intact. After 4 weeks of immobilization, fibroblast membranes in the anterior joint capsule exhibited disrupted integrity and intracellular leakage. While 4 weeks of natural recovery yielded minimal improvement in this pathological state, a subsequent 4-week course of ESW therapy partially restored the structural integrity of these fibroblast membranes. These findings indicate that ESW may mitigate the abnormal pyroptosis caused by fixation in the anterior joint capsule, and this suppression likely contributes to the treatment's anti-fibrotic effects.

MCC950 is a well-established NLRP3 inhibitor that prevents the activation of the NLRP3 inflammasome in diverse pathological states, thereby suppressing NLRP3-dependent pyroptosis [39,40,41,42]. To further elucidate the role of pyroptosis in joint contracture, we assessed whether NLRP3 inhibition via MCC950 could ameliorate pyroptosis, fibrosis, and subsequent contracture. The results suggest that MCC950 intervention can inhibit pyroptosis, limit fibrosis, and decrease the severity of knee joint contracture. Notably, groups with higher pyroptosis marker expression (e.g., Groups M and NR) consistently exhibited more severe joint contracture and collagen deposition, whereas groups with lower pyroptosis levels (e.g., Groups E and MCC950) showed milder pathological changes, suggesting a close association between pyroptosis activation and the severity of fibrosis and contracture. Group-mean correlation analysis also showed that pyroptosis is closely

linked to arthrogenic contracture and Masson collagen deposition. Although this exploratory analysis is based on group-level means rather than individual-animal molecular data, it provides quantitative support for the proposed mechanism whereby pyroptosis activation is linked to more severe capsular fibrosis and joint stiffness. These findings further validate that stimulating pyroptosis in the joint capsule may drive the progression of knee joint contractures in rats.

To further investigate how a hypoxic environment influences pyroptosis and fibrosis, rat knee synovial fibroblasts were used as the primary cell model in this study. The transformation of fibroblasts into myofibroblasts represents a crucial stage in the process of fibrosis [43]. Moreover, α-SMA is a key molecule reflecting the differentiation of myofibroblasts. In this study, hypoxia induced the upregulation of α-SMA, an effect that was most pronounced after 24 hours. Meanwhile, exposing rat knee synovial fibroblasts to hypoxia for 6, 12, or 24 h led to a time-dependent decrease in cell viability. Since cell viability did not significantly differ between 12 h and 24 h exposure, 24 h was subsequently used to induce hypoxia for subsequent studies on pyroptosis and fibrosis in rat knee synovial fibroblasts. These findings demonstrated that hypoxia upregulated HIF-1α, leading to higher levels of both pyroptosis and fibrotic markers. Conversely, HIF-1α siRNA suppressed these effects, lowering the expression of proteins linked to both pyroptosis and fibrosis. Additionally, FAM-YVAD-FMK/PI staining was utilized to detect pyroptosis levels, yielding results that aligned with our earlier protein examination data. These findings demonstrated that hypoxic conditions markedly upregulated pyroptosis and fibrosis in myofibroblasts. However, HIF-1α siRNA intervention effectively mitigated pyroptosis. Together, these results confirm that hypoxia promotes pyroptosis and accelerates fibrosis progression in synovial fibroblasts. The research further indicated that ESW might mitigate fibrosis by modulating local hypoxia within the joint capsule, which leads to the downregulation of HIF-1α expression. Subsequently, this reduction inhibits abnormally activated pyroptosis.

Limitations

Several limitations of this study should be acknowledged. First, the observation period was limited to 4 weeks after ESW treatment; thus, long-term follow-up studies are needed to determine the durability of the therapeutic effects and rule out potential late adverse events. Second, all *in vivo* experiments were restricted to male rat models, which overlooks potential sex-dependent differences in fibrotic and inflammatory mechanisms. Consequently, the applicability of these conclusions to females remains underdetermined. Therefore, future studies should incorporate female rats to establish the generalizability of these findings, and further validations should be conducted using other species or human tissue samples. Third, although our loss-of-function data (using *in vivo* MCC950 and *in vitro* HIF-1α siRNA) indicate involvement of the HIF-1α/NLRP3/pyroptosis axis, we did not conduct *in vivo* rescue experiments (e.g., overexpression of HIF-1α or activation of NLRP3 during ESW). Such direct validation is a crucial step for future research to confirm this causal relationship. Fourth, our functional assessment was limited to ROM measurement; additional assessments such as gait analysis and weight-bearing tests need to be carried out to provide a more comprehensive functional evaluation in the future. Lastly, because of their shared fibrotic responses in hypoxic environments, synovial fibroblasts were utilized in our *in vitro* experiments as a surrogate for joint capsular fibroblasts. To build upon these findings, further research must validate these results using primary joint capsular fibroblasts. Furthermore, future research should extend the observation periods, feature both sexes and diverse animal models, include *in vivo* rescue experiments, and incorporate additional functional assessments.

5. Conclusions

In conclusion, our findings suggest that ESW can effectively improve immobilization-induced contracture. The therapeutic benefits appear to be mediated by the amelioration of the tissue hypoxia environment and the suppression of pyroptosis within the joint capsule tissues. While promising in rat models, further validation in diverse animal models and human tissues is required before clinical application.

Availability of Data and Materials

The data supporting the findings of this study are available from the corresponding author upon reasonable request. Neither the manuscript nor any of its contents has been published previously or is currently under consideration for publication elsewhere.

Author Contributions

QBZ designed and coordinated the study, conducted the molecular experiments, and prepared the manuscript. XML, XLK and FW participated in the design and statistical analysis. LH conducted the animal experiments. AYL carried out the molecular studies. ML took part in the development of the mechanical goniometer. QQB participated in the molecular studies. RZ, DTZ and ZYD carried out the pathological studies. JM and YZ contributed to the study's design, coordination, and manuscript preparation. All authors have participated in the drafting and critical revision of the manuscript for important intellectual content. All authors read and approved the final manuscript. All authors have participated sufficiently in the work and agreed to be accountable for all aspects of the work.

Ethics Approval and Consent to Participate

All animal care and experimental operations were carried out in strict compliance with the Guidelines for Animal Experimentation of Anhui Medical University and had obtained the approval from the Institutional Animal Care and Use Committee (NO. LLSC20221126). The study was reported in accordance with the ARRIVE guidelines 2.0.

Acknowledgment

We are deeply thankful for the valuable guidance and kind assistance provided by Associate Professor Hua-Long Zhu from the School of Public Health at Anhui Medical University and Professor Bin Li from Soochow University.

Funding

This work was supported by Anhui Provincial Natural Science Foundation (2408085QH270); Health Research Program of Anhui (AHWJ2023A30077); Summit Discipline Construction Project of Anhui Medical University (Clinical Medicine) in 2022 (2022GFXK-EFY08); Clinical Medicine Discipline Construction Project of Anhui Medical University in 2023 (2023lcxkEFY010); National Natural Science Incubation Program of the Second Hospital of Anhui Medical University (2022GMFY05); Research Fund of Anhui Institute of translational medicine (2023zhyx-C85); Key Natural Science Research Project of Anhui Educational Committee (2024AH050788).

Conflicts of Interest

The authors declare no conflicts of interest

Supplementary Material

Supplementary material associated with this article can be found, in the online version, at https://doi.org/10.31083/FBL52155.

References

[1] Li Y, Liao Q, Zeng J, Zhang Z, Li B, Luo Z, et al. Extracorporeal Shock Wave Therapy Improves Nontraumatic Knee Contracture in a Rat Model. Clinical Orthopaedics and Related Research. 2023; 481: 822–834. https://doi.org/10.1097/CORR.0000000000002559

[2] Wegner E, Warnke D, Buschmann V, Hild B, Mais B, Ritz U, et al. Nintedanib reduces severity of post-traumatic joint contracture by modulating fibrosis and inflammation. Journal of Molecular Medicine. 2025; 103: 1461–1474. https://doi.org/10.1007/s00109-025-02593-2

[3] Zhang QB, Huo L, Li M, Zhang R, Zhou T, Wang F, et al. Role of hypoxia-mediated pyroptosis in the development of extending knee joint contracture in rats. European Journal of Medical Research. 2024; 29: 298. https://doi.org/10.1186/s40001-024-01890-9

[4] Liao CD, Xie GM, Tsauo JY, Chen HC, Liou TH. Efficacy of extracorporeal shock wave therapy for knee tendinopathies and other soft tissue disorders: a meta-analysis of randomized controlled trials. BMC Musculoskeletal Disorders. 2018; 19: 278. https://doi.org/10.1186/s12891-018-2204-6

[5] Ryskalin L, Morucci G, Natale G, Soldani P, Gesi M. Molecular Mechanisms Underlying the Pain-Relieving Effects of Extracorporeal Shock Wave Therapy: A Focus on Fascia Nociceptors. Life (Basel, Switzerland). 2022; 12: 743. https://doi.org/10.3390/life12050743

[6] Stania M, Juras G, Chmielewska D, Polak A, Kucio C, Król P. Extracorporeal Shock Wave Therapy for Achilles Tendinopathy. BioMed Research International. 2019; 2019: 3086910. https://doi.org/10.1155/2019/3086910

[7] Sorg H, Zwetzich I, Tilkorn DJ, Kolbenschlag J, Hauser J, Goertz O, et al. Effects of Extracorporeal Shock Waves on Microcirculation and Angiogenesis in the in vivo Wound Model of the Diver Box. European Surgical Research. 2021; 62: 134–143. https://doi.org/10.1159/000515737

[8] Wang F, Li W, Zhou Y, Huang PP, Zhang QB. Radial extracorporeal shock wave reduces myogenic contracture and muscle atrophy via inhibiting NF-κB/HIF-1α signaling pathway in rabbit. Connective Tissue Research. 2022; 63: 298–307. https://doi.org/10.1080/03008207.2021.1920934

[9] Hu C, Zhang QB, Wang F, Wang H, Zhou Y. The effect of extracorporeal shock wave on joint capsule fibrosis in rats with knee extension contracture: a preliminary study. Connective Tissue Research. 2023; 64: 469–478. https://doi.org/10.1080/03008207.2023.2217254

[10] Deng M, Zhang W, Yuan L, Tan J, Chen Z. HIF-1a regulates hypoxia-induced autophagy via translocation of ANKRD37 in colon cancer. Experimental Cell Research. 2020; 395: 112175. https://doi.org/10.1016/j.yexcr.2020.112175

[11] Zhang X, Cao W, Pan M, Huo J, Zhang N, Guo J, et al. Huangqi Baihe Granules Attenuate Hypobaric Hypoxia-Induced Brain Injury via HIF-1a/p53/Caspase-3 Pathway. Drug Design, Development and Therapy. 2025; 19: 8823–8841. https://doi.org/10.2147/DDDT.S525602

[12] Gan C, Cai Q, Tang C, Gao J. Inflammasomes and Pyroptosis of Liver Cells in Liver Fibrosis. Frontiers in Immunology. 2022; 13: 896473. https://doi.org/10.3389/fimmu.2022.896473

[13] Zhou Z, Li Q. The Role of Pyroptosis in the Pathogenesis of Kidney Diseases. Kidney Diseases (Basel, Switzerland). 2023; 9: 443–458. https://doi.org/10.1159/000531642

[14] Xiao Y, Zhao C, Tai Y, Li B, Lan T, Lai E, et al. STING mediates hepatocyte pyroptosis in liver fibrosis by Epigenetically activating the NLRP3 inflammasome. Redox Biology. 2023; 62: 102691. https://doi.org/10.1016/j.redox.2023.102691

[15] Huo L, Zhang QB, Zhu DT, Wang K, Du ZY, Li XM, et al. Preliminary study of extracorporeal shock wave alleviating joint capsule fibrosis caused by internal bleeding of knee joint in rats. Connective Tissue Research. 2024; 65: 397–406. http://doi.org/10.1080/03008207.2024.2387729

[16] Zhang C, Huang Y, Ouyang F, Su M, Li W, Chen J, et al. Extracellular vesicles derived from mesenchymal stem cells alleviate neuroinflammation and mechanical allodynia in interstitial cystitis rats by inhibiting NLRP3 inflammasome activation. Journal of Neuroinflammation. 2022; 19: 80. https://doi.org/10.1186/s12974-022-02445-7

[17] Kaneguchi A, Ozawa J, Minamimoto K, Yamaoka K. A rat model of arthrofibrosis developed after anterior cruciate ligament reconstruction without rigid joint immobilization. Connective Tissue Research. 2021; 62: 263–276. https://doi.org/10.1080/03008207.2019.1693548

[18] Li XM, Wang K, Liu M, Zhang QB, Zhou Y. Nicorandil mitigates arthrogenic contracture induced by knee joint extension immobilization in rats: interference with RhoA/ROCK signaling and TGF-β1/Smad pathway. European Cells & Materials. 2024; 47: 59–72. http://doi.org/10.22203/eCM.v047a05

[19] Jun JH, Park GY, Chae CS, Suh DC. The Effect of Extracorporeal Shock Wave Therapy on Pain Intensity and Neck Disability for Patients With Myofascial Pain Syndrome in the

Neck and Shoulder: A Meta-Analysis of Randomized Controlled Trials. American Journal of Physical Medicine & Rehabilitation. 2021; 100: 120–129. https://doi.org/10.1097/PHM.0000000000001493

[20] Menekseoglu AK, Korkmaz MD, Segmen H. Clinical and electrophysiological efficacy of extracorporeal shock-wave therapy in carpal tunnel syndrome: a placebo-controlled, double-blind clinical trial. Revista Da Associacao Medica Brasileira (1992). 2023; 69: 124–130. https://doi.org/10.1590/1806-9282.20220943

[21] Ujiie N, Nakano T, Yamada M, Sato C, Nakanishi C, Fujishima F, et al. Low-energy extracorporeal shock wave therapy for a model of liver cirrhosis ameliorates liver fibrosis and liver function. Scientific Reports. 2020; 10: 2405. https://doi.org/10.1038/s41598-020-58369-w

[22] Zhao JC, Zhang BR, Hong L, Shi K, Wu WW, Yu JA. Extracorporeal shock wave therapy with low-energy flux density inhibits hypertrophic scar formation in an animal model. International Journal of Molecular Medicine. 2018; 41: 1931–1938. https://doi.org/10.3892/ijmm.2018.3434

[23] Salib CG, Reina N, Trousdale WH, Limberg AK, Tibbo ME, Jay AG, et al. Inhibition of COX-2 Pathway as a Potential Prophylaxis Against Arthrofibrogenesis in a Rabbit Model of Joint Contracture. Journal of Orthopaedic Research : Official Publication of the Orthopaedic Research Society. 2019; 37: 2609–2620. https://doi.org/10.1002/jor.24441

[24] Reiter AJ, Schott HR, Castile RM, Cannon PC, Havlioglu N, Chamberlain AM, et al. Early Joint Use Following Elbow Dislocation Limits Range-of-Motion Loss and Tissue Pathology in Posttraumatic Joint Contracture. The Journal of Bone and Joint Surgery. American Volume. 2023; 105: 223–230. https://doi.org/10.2106/JBJS.22.00064

[25] Wynn TA, Ramalingam TR. Mechanisms of fibrosis: therapeutic translation for fibrotic disease. Nature Medicine. 2012; 18: 1028–1040. https://doi.org/10.1038/nm.2807

[26] Zuo S, Wang B, Liu J, Kong D, Cui H, Jia Y, et al. ER-anchored CRTH2 antagonizes collagen biosynthesis and organ fibrosis via binding LARP6. The EMBO Journal. 2021; 40: e107403. https://doi.org/10.15252/embj.2020107403

[27] Andugulapati SB, Gourishetti K, Tirunavalli SK, Shaikh TB, Sistla R. Biochanin-A ameliorates pulmonary fibrosis by suppressing the TGF-β mediated EMT, myofibroblasts differentiation and collagen deposition in in vitro and in vivo systems. Phytomedicine : International Journal of Phytotherapy and Phytopharmacology. 2020; 78: 153298. https://doi.org/10.1016/j.phymed.2020.153298

[28] Yabe Y, Hagiwara Y, Suda H, Ando A, Onoda Y, Tsuchiya M, et al. Joint immobilization induced hypoxic and inflammatory conditions in rat knee joints. Connective Tissue Research. 2013; 54: 210–217. https://doi.org/10.3109/03008207.2013.786056

[29] Yuan D, Guan S, Wang Z, Ni H, Ding D, Xu W, et al. HIF-1α aggravated traumatic brain injury by NLRP3 inflammasome-mediated pyroptosis and activation of microglia. Journal of Chemical Neuroanatomy. 2021; 116: 101994. https://doi.org/10.1016/j.jchemneu.2021.101994

[30] Hong Z, Zhang X, Zhang T, Hu L, Liu R, Wang P, et al. The ROS/GRK2/HIF-1α/NLRP3 Pathway Mediates Pyroptosis of Fibroblast-Like Synoviocytes and the Regulation of Monomer Derivatives of Paeoniflorin. Oxidative Medicine and Cellular Longevity. 2022; 2022: 4566851. https://doi.org/10.1155/2022/4566851

[31] Zhou L, Zhang H, Liu L, Zhang F, Wang L, Zheng P, et al. Intermittent hypoxia aggravates asthma inflammation via NLRP3/IL-1β-dependent pyroptosis mediated by HIF-1α signalling pathway. Chinese Medical Journal. 2025; 138: 1714–1729. https://doi.org/10.1097/CM9.0000000000003608

[32] Wang Y, Wu W, Xu Y, Wu C, Han Q, Lu T, et al. Ncl liquid-liquid phase separation and SUMOylation mediate the stabilization of HIF-1α expression and promote pyroptosis in ischemic hindlimb. Biochimica et Biophysica Acta. Molecular Basis of Disease. 2025; 1871: 167706. https://doi.org/10.1016/j.bbadis.2025.167706

[33] Shi J, Zhang Z, Zhang W, Zhao X. Mechanism of the DDX3X/NLRP3/GSDMD Signaling Axis in Pyroptosis and Inflammatory Response in Osteoarthritis Chondrocytes. Journal of Biochemical and Molecular Toxicology. 2026; 40: e70618. https://doi.org/10.1002/jbt.70618

[34] Panganiban RA, Nadeau KC, Lu Q. Pyroptosis, gasdermins and allergic diseases. Allergy. 2024; 79: 2380–2395. https://doi.org/10.1111/all.16236

[35] Wright SS, Kumari P, Fraile-Ágreda V, Wang C, Shivcharan S, Kappelhoff S, et al. Transplantation of gasdermin pores by extracellular vesicles propagates pyroptosis to bystander cells. Cell. 2025; 188: 280–291.e17. https://doi.org/10.1016/j.cell.2024.11.018

[36] Sun Y, Li F, Liu Y, Qiao D, Yao X, Liu GS, et al. Targeting inflammasomes and pyroptosis in retinal diseases-molecular mechanisms and future perspectives. Progress in Retinal and Eye Research. 2024; 101: 101263. https://doi.org/10.1016/j.preteyeres.2024.101263

[37] Gao J, Peng S, Shan X, Deng G, Shen L, Sun J, et al. Inhibition of AIM2 inflammasome-mediated pyroptosis by Andrographolide contributes to amelioration of radiation-induced lung inflammation and fibrosis. Cell Death & Disease. 2019; 10: 957. https://doi.org/10.1038/s41419-019-2195-8

[38] Gaul S, Leszczynska A, Alegre F, Kaufmann B, Johnson CD, Adams LA, et al. Hepatocyte pyroptosis and release of inflammasome particles induce stellate cell activation and liver fibrosis. Journal of Hepatology. 2021; 74: 156–167. https://doi.org/10.1016/j.jhep.2020.07.041

[39] Coll RC, Hill JR, Day CJ, Zamoshnikova A, Boucher D, Massey NL, et al. MCC950 directly targets the NLRP3 ATP-hydrolysis motif for inflammasome inhibition. Nature Chemical Biology. 2019; 15: 556–559. https://doi.org/10.1038/s41589-019-0277-7

[40] Zeng W, Wu D, Sun Y, Suo Y, Yu Q, Zeng M, et al. The selective NLRP3 inhibitor MCC950 hinders atherosclerosis development by attenuating inflammation and pyroptosis in macrophages. Scientific Reports. 2021; 11: 19305. https://doi.org/10.1038/s41598-021-98437-3

[41] Ward R, Li W, Abdul Y, Jackson L, Dong G, Jamil S, et al. NLRP3 inflammasome inhibition with MCC950 improves diabetes-mediated cognitive impairment and vasoneuronal remodeling after ischemia. Pharmacological Research. 2019; 142: 237–250. https://doi.org/10.1016/j.phrs.2019.01.035

[42] Li H, Wang X, Luo X, Shi H, Li J. cGAS/STING/NLRP3 Signaling Pathway-Mediated Pyroptosis in Hypertrophic Cardiomyopathy Radiotherapy. Frontiers in Bioscience (Landmark Edition). 2025; 30: 26084. https://doi.org/10.31083/FBL26084

[43] Wu D, Jiang M, Zhang J. Dual Role of Quercetin in Promoting Early Wound Healing via Inhibiting Inflammatory Factors and Attenuating Scar Formation by Suppressing Myofibroblast Differentiation. Frontiers in Bioscience (Landmark Edition). 2025; 30: 40077. https://doi.org/10.31083/FBL40077